Biosensors and Bioelectronics 261 (2024) 116466

Contents lists available at ScienceDirect

Biosensors and Bioelectronics

journal homepage: www.elsevier.com/locate/bios

Precision detection of select human lung cancer biomarkers and cell lines using honeybee olfactory neural circuitry as a novel gas sensor

Michael Parnas [a,1], Autumn K. McLane-Svoboda [a,1], Elyssa Cox [a,1], Summer B. McLane-Svoboda [a], Simon W. Sanchez [a], Alexander Farnum [a], Anthony Tundo [a], Noël Lefevre [a], Sydney Miller [a], Emily Neeb [a], Christopher H. Contag [a,b], Debajit Saha [a,c,*]

[a] Department of Biomedical Engineering and the Institute for Quantitative Health Science and Engineering, Michigan State University, East Lansing, MI, USA
[b] Department of Microbiology, Genetics & Immunology, Michigan State University, East Lansing, MI, USA
[c] Neuroscience Program, Michigan State University, East Lansing, MI, USA

A B S T R A C T

Human breath contains biomarkers (odorants) that can be targeted for early disease detection. It is well known that honeybees have a keen sense of smell and can detect a wide variety of odors at low concentrations. Here, we employ honeybee olfactory neuronal circuitry to classify human lung cancer volatile biomarkers at different concentrations and their mixtures at concentration ranges relevant to biomarkers in human breath from parts-per-billion to parts-per-trillion. We also validated this brain-based sensing technology by detecting human non-small cell lung cancer (NSCLC) and small cell lung cancer (SCLC) cell lines using the 'smell' of the cell cultures. Different lung cancer biomarkers evoked distinct spiking response dynamics in the honeybee antennal lobe neurons indicating that those neurons encoded biomarker-specific information. By investigating lung cancer biomarker-evoked population neuronal responses from the honeybee antennal lobe, we classified individual human lung cancer biomarkers successfully (88% success rate). When we mixed six lung cancer biomarkers at different concentrations to create 'synthetic lung cancer' vs. 'synthetic healthy' human breath, honeybee population neuronal responses were able to classify those complex breath mixtures reliably with exceedingly high accuracy (93–100% success rate with a leave-one-trial-out classification method). Finally, we employed this sensor to detect human NSCLC and SCLC cell lines and we demonstrated that honeybee brain olfactory neurons could distinguish between lung cancer vs. healthy cell lines and could differentiate between different NSCLC and SCLC cell lines successfully (82% classification success rate). These results indicate that the honeybee olfactory system can be used as a sensitive biological gas sensor to detect human lung cancer.

1. Introduction

Honeybees have a sensitive olfactory system designed to help them navigate complex environments encompassing foraging, reproduction, brood care, and defense. Consequently, they can be used to reliably detect a wide range of volatile chemicals, or the 'smell' of objects, while also distinguishing between odor mixtures efficiently even at low concentrations (Moreno et al., 2022; Reinhard et al., 2010; Sandoz, 2011; Bortolotti and Costa, 2014). Here, we hypothesize that the honeybee's powerful olfactory neural circuitry can be leveraged to develop a gas sensing system with the ability to detect lung cancer biomarkers present in exhaled human breath and differentiate between various non-small cell and small cell human lung cancers.

Lung cancer is the second most commonly diagnosed cancer worldwide and is the leading cause of cancer-related death among both men and women (Sung et al., 2021). It can be divided into two main types, (1) non-small cell lung cancer (NSCLC) and (2) small cell lung cancer (SCLC), each of which has different morphologic and metabolomic characteristics (Kowalczyk et al., 2021; Lim et al., 2018). NSCLC are larger cells that grow slower, whereas SCLC are smaller cancer cells that can proliferate and metastasize quickly (Pedersen et al., 2021). The alterations of cell growth and movement may be related to metabolic differences between the two types. Cancers are shown to have different concentrations of metabolic substrates compared to healthy cells and other sub-types of cancer (Pedersen et al., 2021;(Staal-van den Brekel, 1997). These differences in metabolism between NSCLC and SCLC can alter the VOCs produced by the cells (Kowalczyk et al., 2021; Pedersen et al., 2021).

Additionally, the analysis of volatile organic compounds (VOCs) in exhaled human breath is a promising approach for detecting metabolic

* Corresponding author. Department of Biomedical Engineering and The Institute for Quantitative Health Science and Engineering, Michigan State University, East Lansing, MI, USA.
E-mail address: sahadeb3@msu.edu (D. Saha).
[1] These authors contributed equally to this manuscript.

https://doi.org/10.1016/j.bios.2024.116466
Received 4 October 2023; Received in revised form 24 May 2024; Accepted 2 June 2024
Available online 4 June 2024

aberrations in diseases such as cancer at an early stage (Gouzerh et al., 2022; Fuchs et al., 2010; Hakim et al., 2011; Nardi-Agmon and Peled, 2017; Peng et al., 2010a; Phillips et al., 1999, 2003, 2006; Raspagliesi et al., 2020; Roine et al., 2014). Therefore, breath-based VOC analysis can potentially address the critical unmet need for sensitive, early, and noninvasive cancer diagnostics (Queralto et al., 2014; Filipiak et al., 2014). Exhaled human breath contains over 3500 known VOCs (Queralto et al., 2014; Ma et al., 2023; Popov, 2011). Different diseases alter the components and concentrations of these VOCs, and thus can reflect the metabolic condition, or health, of an individual (Nardi-Agmon and Peled, 2017; Gruber et al., 2014; Lim et al., 2014; Mochalski et al., 2018; Phillips et al., 2020). Several studies employing exhaled human breath and mass spectrometry have shown that cancer can alter specific VOCs in exhaled breath at parts-per-billion (ppb) to parts-per-trillion (ppt) ranges (Fuchs et al., 2010; Filipiak et al., 2014). In this study, we focus on VOCs that are known to be altered in patients with lung cancer through the analysis of synthetic human breath and cultured human lung cancer cell lines. Studies using different variations of mass spectrometry have shown that VOCs produced by cancer cells are different from those produced by normal cells *in vitro* (Thriumani et al., 2016, 2018; Jia et al., 2018; Serasanambati et al., 2019a; Furuhashi et al., 2020; Davies et al., 2014; Peled et al., 2013; Brunner et al., 2010; Sponring et al., 2010; Barash et al., 2012). The headspace over cultured cells have specific VOC compositions that correspond to the cancer type, including breast cancer (He et al., 2014; Lavra et al., 2015; Silva et al., 2017), liver cancer (Amal et al., 2012; Mochalski et al., 2013), prostate cancer (Lima et al., 2018), gastric cancer (Zhang et al., 2014), leukemia (Tang et al., 2017), and lung cancer (Choueiry et al., 2022; Choueiry and Zhu, 2022; Janssens et al., 2022).

Analytical techniques including most notably gas chromatography mass spectrometry (GC-MS) (Nardi-Agmon and Peled, 2017; Gruber et al., 2014; Lim et al., 2014; Mochalski et al., 2018; Saidi et al., 2020; Altomare et al., 2013, 2020; Amal et al., 2015, 2016; Guo et al., 2015; Schallschmidt et al., 2016; Wang et al., 2014; Koureas et al., 2020), but also selected-ion flow-tube mass spectrometry (SIFT-MS) (Španěl and Smith, 2020), proton transfer reaction mass spectrometry (PTR-MS) (Brunner et al., 2010), gas chromatography ion mobility spectrometry (GC-IMS) (Chen et al., 2021; Tiele et al., 2019, 2020), and field asymmetric ion mobility spectrometry (FAIMS) (Arasaradnam et al., 2014, 2018; Niemi et al., 2018) have been used for disease detection via VOC analysis (Gouzerh et al., 2022; Pereira et al., 2015a; Kaloumenou et al., 2022). Although, GC-MS, the current gold standard, has high sensitivity and specificity when identifying known compounds, it has difficulty in identifying correct concentrations of unknown compounds at ppb to ppt levels and requires pre- and post-processing of data, which is not standardized. Another technology for VOC sensing is electronic noses (e-noses) which employ some biological principles for one-shot gas sensing. These e-nose devices are portable and can detect a few target compounds at low (ppb) concentrations. E-nose devices have been successfully employed to detect multiple types of cancer (Raspagliesi et al., 2020; Roine et al., 2014; Amal et al., 2016; Broza et al., 2019; Chang et al., 2018; Díaz De León-Martínez et al., 2020; Kononov et al., 2019; Krauss et al., 2020; Van De Goor et al., 2018; van de Goor et al., 2017; van Keulen et al., 2020; Waltman et al., 2020; Barash et al., 2015; Chen et al., 2016; Peng et al., 2009, 2010b; Shehada et al., 2015). However, e-noses are usually targeted for a specific chemical, and these engineered sensors cannot match the broad sensitivity and specificity of biological chemical sensors (Karakaya et al., 2020; Lüdke and Galizia, 2014; Hurot et al., 2020; Brooks et al., 2015; Scheepers et al., 2022; Baldini et al., 2020; Manzini et al., 2021).

Biological "noses," such as the honeybee antennae and olfactory brain are extremely sensitive, and honeybees have been shown to learn odor identity and perform complex olfactory behavioral tasks (Moreno et al., 2022; Sandoz, 2011; Chen et al., 2015). Similar to dogs' noses which have been successful in the detection of different VOCs of interests (Lüdke and Galizia, 2014; Cornu et al., 2011; Willis et al., 2004a, 2011; Amundsen et al., 2014; Horváth et al., 2009; Urbanová et al., 2015; Williams and Pembroke, 1989), it has been demonstrated that insects' noses, or antennae, can be exposed to a target smell and reinforced with a food reward for detection of that target stimuli, behaviorally (Bitterman et al., 1983). Here, we take advantage of the honeybees' sensitive olfactory system to test whether the central olfactory neural circuitry (i.e., the antennal lobe) can generate discriminatory neural responses to single human lung cancer biomarkers, mixtures of these VOCs as simulated breath, as well as VOC mixtures emitted from cultures of human lung cancer cells. In the honeybee olfactory sensory pathway, olfactory receptor neurons (ORNs), located in the antenna convert chemical cues into electrical signals. Briefly, VOCs from the environment can enter small hair-like follicles (sensilla) on the antennal surface through small pores. Once within the sensilla lymph, olfactory binding proteins (OBP) bind to the VOCs and transport them to the ORNs. Olfactory receptors on the ORN membranes react with specific VOC/OBP complexes to change the membrane electrical potential which can lead to an action potential (Yang et al., 2012; Brito et al., 2016). These action potentials act as information packets and travel from ORNs to the antennal lobe where two types of neurons, projection neurons (PNs) and local neurons (LNs), form dense clusters of connections called glomeruli. Each glomerulus is activated by ORNs that express a single type of olfactory receptor. Based on a combinatorial coding scheme and the roughly 170 glomeruli within the antennal lobe, honeybees can theoretically differentiate between $\sim 2^{170}$ odors (Sachse et al., 1999; Brill et al., 2013; Robertson and Wanner, 2006). The roughly 60,000 ORNs present in the honeybee antenna send their output to only 800 PNs in the antennal lobe (MaBouDi et al., 2017), which transmit odor-evoked spiking responses to 368,000 Kenyon cells in the mushroom body (Groh and Rössler, 2020), making the antennal lobe an ideal location for neural recordings due to the convergence of VOC-evoked spiking information. The network of PNs and LNs uniquely respond to odor identity and concentration in a highly replicable manner (Stopfer et al., 2003). This response is akin to a fingerprint, or template. Neural responses to unknown odors can be compared with these templates for odor identification (Figs. 1–4).

In this study, we have systematically tested three hypotheses: (1) honeybee antennal lobe neurons (ALNs) possess discriminatory information corresponding to multiple human lung cancer biomarkers, (2) these neurons can differentiate between small differences in concentrations of the lung cancer biomarker mixtures (i.e., synthetic lung cancer vs. synthetic healthy breath mixtures), and (3) this sensing approach can detect various human lung cancer cell lines based on their 'smell'. To achieve these goals, we have performed *in vivo* electrophysiological recordings from the honeybee antennal lobe while exposing the honeybee antennae to lung cancer biomarkers at a variety of concentrations, synthetic mixtures of these biomarkers, and natural VOC mixtures present in the headspace of human lung cancer cell cultures. We analyzed the VOC-evoked neural data using biological neural computational schemes to classify lung cancer and to test our hypotheses.

2. Results

2.1. Human lung cancer biomarkers are detected by the neurons in the honeybee antennal lobe

We obtained individual lung cancer VOC-evoked neural responses from the honeybee antennal lobe circuit. The rationale for targeting antennal lobe circuitry was twofold: (1) since 60,000 ORNs from the antennae converge to only 800 PNs in the honeybee antennal lobe, the probability of getting odor evoked responses to diverse VOCs is higher from the ALN recordings, and (2) in the honeybee antennal lobe, spatiotemporal response properties of ALNs are odor specific (Krofczik et al., 2009; Joerges et al., 1997). We chose nine different VOCs which are implicated as human exhaled breath lung cancer biomarkers (Phillips et al., 1999; Poli et al., 2010). For these sets of experiments, the

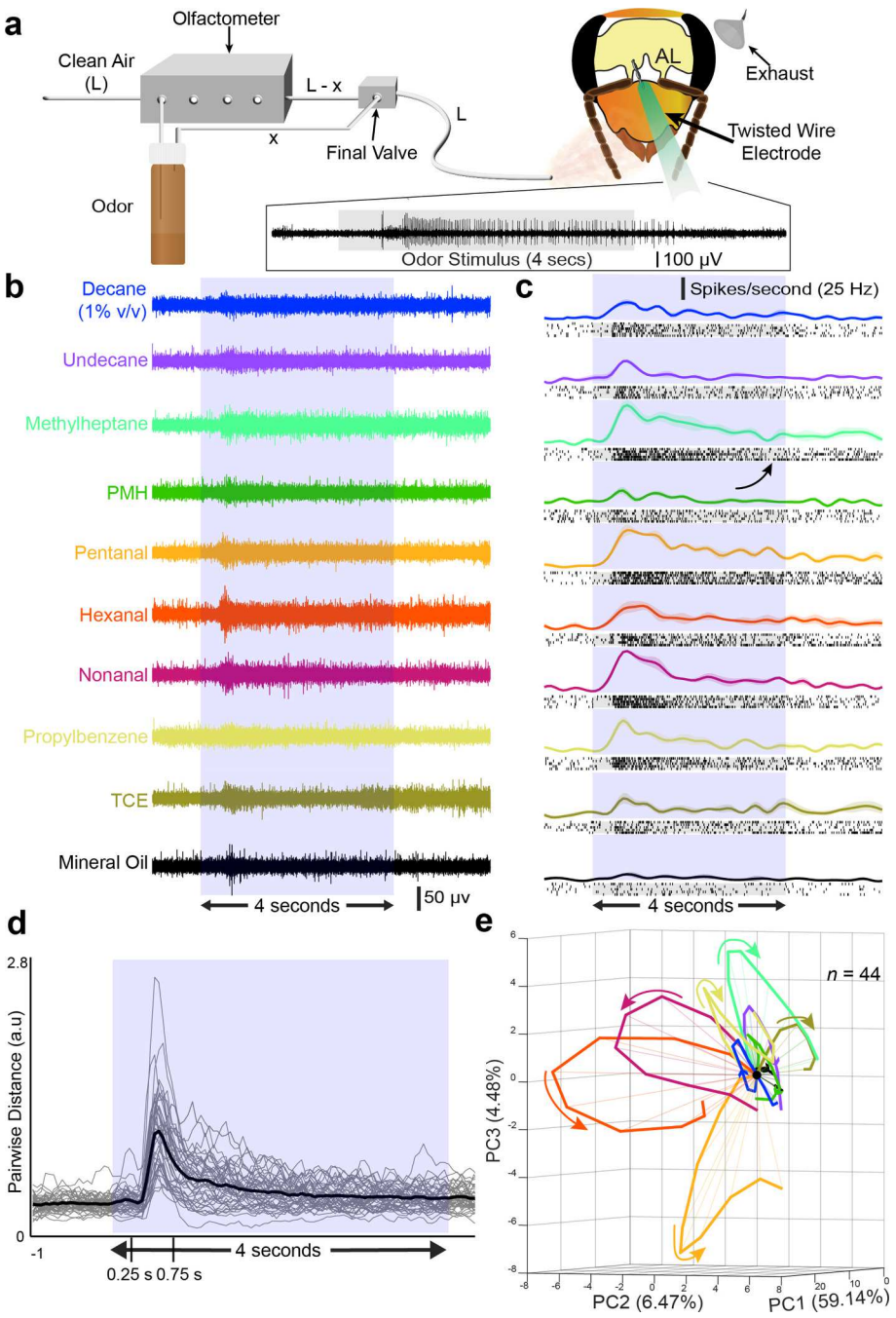

Fig. 1. Individual neurons display distinct odor evoked responses to putative lung cancer biomarkers. (a) Schematic of the experimental setup. Starting from the left, clean air from a compressed air cylinder enters an olfactometer with a flow rate, L. Prior to odor stimulus, the entire flow rate, L, is delivered directly to the honeybee's antennae. When the odor stimulus starts, the olfactometer diverts a portion of the air, x, into the headspace of an odor vial that contains a single VOC mixed with mineral oil (1% v/v). The clean air (L-x) and the odor laden air (x) are combined at the final valve and delivered to the antennae. A custom-built twisted wire electrode placed within the honeybee antennal lobe records the VOC-evoked neural responses (shown at the bottom). **(b)** Representative extracellular lung cancer VOC-evoked neural voltage responses from a recording location within the honeybee antennal lobe is shown. Responses to nine putative cancer biomarkers mixed in mineral oil (1% v/v) as well as a pure mineral oil control-evoked response are shown. The light blue box indicates the odor presentation window (4 s). **(c)** The representative VOC-evoked voltage responses shown in **panel b** were spike sorted and the raster and peri-stimulus time histograms (PSTHs) of one antennal lobe neuron's responses to all 10 odors are shown. Each black line in the raster plot indicates an action potential, or spiking event, from the neuron. Raster plots are shown for all five trials of each VOC presentation. The PSTHs (in color) show the changes in spiking rate over time for the neuron with an increase in firing rate correlated to an increase in density of the raster plots. Trial-averaged PSTHs are plotted with the shaded region indicating the S.E.M. The light blue box in the background indicates the 4 s odor presentation window. **(d)** Pairwise distance plots (see Experimental Section) are shown for all recorded neurons (n = 44 ALNs). Each grey line is the average of all possible pairwise distances from a single neuron's responses to all 10 odors. The black line is the average value of pairwise distances across all 44 neurons. Notice that the average pairwise distances of most neurons have a maximum value during the transient phase of odor stimulus from 0.25 to 0.75 s after stimulus onset. **(e)** VOC-evoked population neural trajectories of all 10 odors are shown using PCA dimensionality reduction. The trajectories are plotted between 0.25 and 0.75 s after stimulus onset to highlight the transient response window, which is the most discriminatory segment of the neural response. The colored arrows indicate the direction of evolution for each VOC-evoked trajectory. All trajectories are aligned at 0.25 s after odor onset (indicated by a black dot), which corresponds to the time of the odor plume hitting the antennae after the opening of the final valve (at 0.0 s).

primary goal was to detect the identity of the volatile chemicals using honeybee neural recordings, therefore, we tested all nine VOCs at a fixed concentration (1% vol/vol, diluted in mineral oil).

The timing and volume of the VOC delivery to the honeybee antennae was carefully controlled while simultaneously conducting *in vivo* extracellular recordings from the ALNs, which contained both PN and LN responses (Fig. 1a). We observed that VOC-evoked neural voltage traces from a single recording site can display different spiking

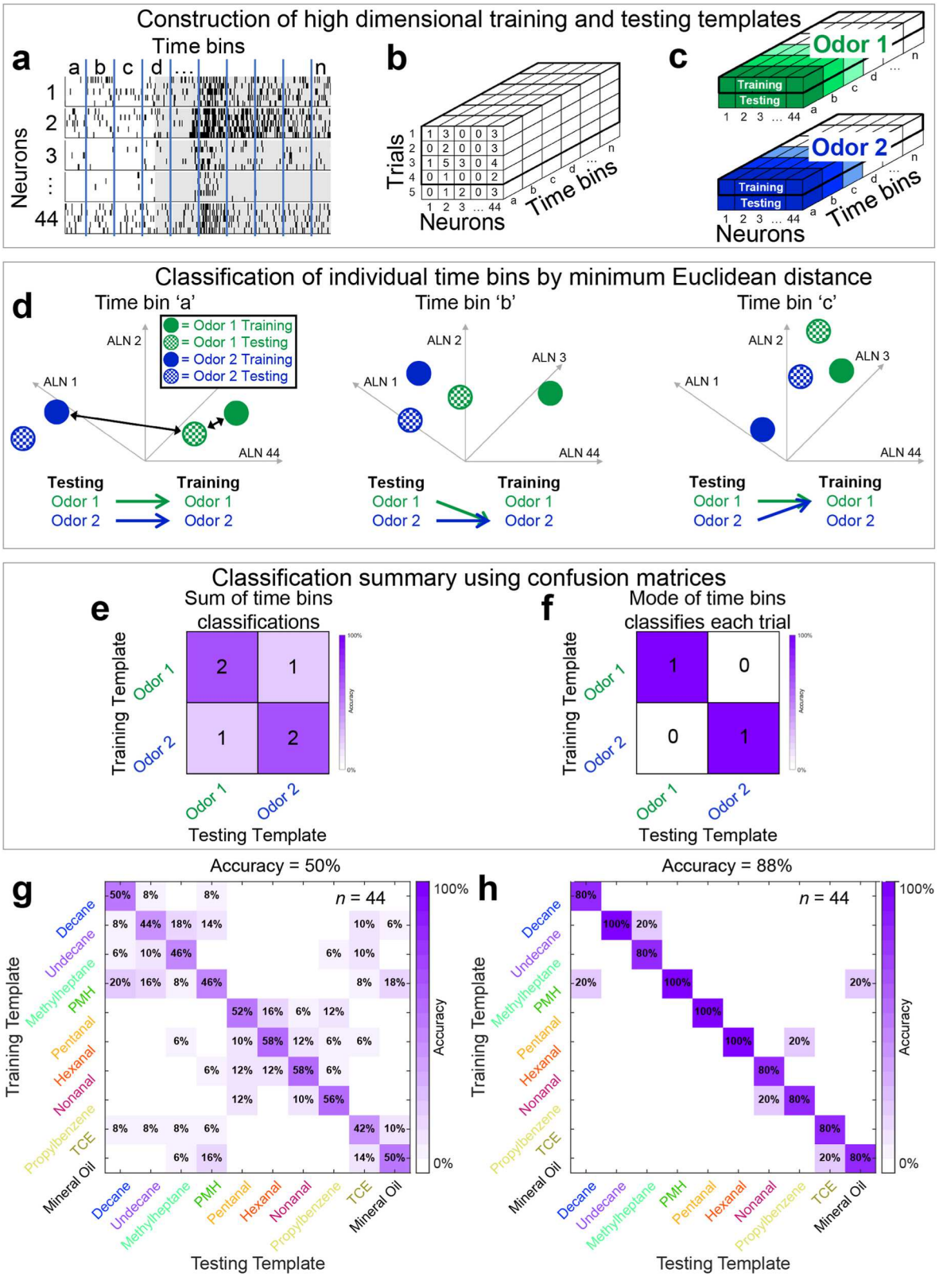

(caption on next page)

Fig. 2. Population neural responses can classify individual lung cancer biomarkers. **(a)** Raster plots of spike sorted neuron responses (1–44) to a single odor (hexanal) from antennal lobe recordings in honeybees. Each neuron's response was recorded for five trials. The responses are all aligned using the stimulus onset as the reference point and binned into discrete, non-overlapping, 50 ms time bins. **(b)** The number of spiking events in each time bin is counted and used to populate a three-dimensional matrix (neurons x trials x time bins). **(c)** Four trials are selected and averaged together to create the training template, with the fifth trial being *left out* to create the testing template, known as a leave-one-trial-out (LOTO) analysis. Each time bin, denoted by the different shades of color, is analyzed separately. **(d)** The training and testing templates for each time bin and both odors, solid and checkered circles, respectively, are visualized as high dimensional points, with the number of dimensions equal to the number of neurons ($n = 44$). Testing templates (checkered) are compared to each training template (solid) and assigned using the smallest Euclidean distance. For *time bin a* (left) the green testing template would be assigned to green, and the blue testing template would be assigned to blue. *Time bin b*, (middle) green is assigned to blue and blue is assigned to blue. *Time bin c*, (right) green is assigned to green and blue is assigned to green. **(e)** Using the previous assignments, a confusion matrix can be populated. The testing templates for each odor are on the x-axis and their assignments are on the y-axis. For two time bins ('a' and 'c'), the green testing template was assigned to green, however for one time bin ('b') green was mis-assigned to blue. We count the assignments for each of the odors. **(f)** Instead of counting each individual bin, the mode of the bin assignments can be used to assign an entire trial. For the left-out trial visualized here, the mode for the green testing template is green (two out of three) and the mode for the blue testing template is blue (two out of three). After completing the analysis for a single left out trial, we can iterate until each trial has been left out once and used as a testing template. Each time using the other four trials to create the training template. And this can be expanded to include any number of odors. **(g)** The count of time bin assignments for all nine VOCs and the mineral oil control shows good classification; notice that the diagonal elements of the confusion matrix show higher values compared to the off-diagonal elements which indicates that testing templates are correctly classified in most cases using this quantitative analysis. Overall success rate of classification for this approach is 50%. **(h)** Instead of classifying each 50 ms bin individually, here, the entire time window between 0.25 and 0.75 s after stimulus onset is being classified in a winner-take-all approach. The mode of the classification value of the 10-time bins (each bin is 50 ms in duration over a total time of 500 ms) was used to determine the overall classification success for the entire testing trial. Using this approach, 44 of the 50 trials were correctly classified with an accuracy of 88%.

response properties to each VOC tested (Fig. 1b). Next, we identified individual ALNs by spike sorting (see Experimental Section) and plotted peri-stimulus time histograms (PSTHs) and raster plots of individual neurons ($n = 44$ ALNs). A representative neuron's odor-evoked responses exhibited distinct differences between all nine VOCs and the mineral oil control (Fig. 1c). Not only can the honeybees detect each of the odors, as shown by the odor-evoked responses, we observed that the ALNs also respond to each odor differently.

Next, we sought to confirm that each ALN contains discriminatory information about odor identity and that the population of ALNs encodes the odors distinctly. To investigate each ALN, we first calculated pairwise distances between all 10 odor-evoked responses and averaged them together for each of the 44 neurons (see Experimental Section, Supplementary Fig. 1). A nonzero pairwise distance plot for a neuron indicates that neuron contains discriminatory information for all stimuli tested. The pairwise distance plots showed that the largest separation of VOC-evoked responses for most neurons occurred during the transient phase of the neural response, which lasts about 1 s from the odor onset (Fig. 1d) (Saha et al., 2013a). We chose a time window from 0.25 to 0.75 s (total 500 ms duration) for data analysis as we found that most neurons responded with a 0.25 s delay from the final olfactometer valve opening. This analysis confirmed that all the neurons in the recorded population contained VOC-specific information which can be used to classify lung cancer VOC identity.

Next, we analyzed the lung cancer biomarker discrimination ability of the entire recorded population of ALNs. To achieve this, multiple neural recordings across honeybees were combined ($n = 44$ ALNs) to generate a lung cancer VOC-evoked population response matrix (*neuron* $\times$ *time*). Odor-evoked responses from every neuron were aligned to the odor onset, trial averaged ($n = 5$ trials) firing rates of each neuron corresponding to each odor were binned into 50 ms nonoverlapping bins and then combined to form time-variant, odor-specific, high dimensional population neuronal response vectors. The 50 ms time window selection corresponds to 20 Hz oscillations of odor-evoked local field potentials observed in insect antennal lobes (Perez-Orive et al., 2002; Stopfer et al., 1997; Stopfer and Laurent, 1999).

To visualize the lung cancer VOC-evoked population neuronal trajectories, a principal component analysis (PCA, see Experimental Section) was performed on the high dimensional neural response dataset. For this analysis, a 500 ms time window was chosen from 0.25 to 0.75 s post-stimulus onset, as the ALNs contained the highest amount of discriminatory information about the odor stimuli during this period (Fig. 1d). PCA was applied on the entire dataset containing all 10 VOCs and the first three principal components with the highest variance were chosen to project the data onto three dimensions for visualization purposes (Fig. 1e). In this reduced space, the odor-evoked population vectors corresponding to each 50 ms time bin were connected in a temporal order to create the neural trajectories for each stimulus and temporally aligned with each other at the origin. Using this analytical technique, previous studies have demonstrated that distinct neural trajectories represent VOC identities and intensities (Stopfer et al., 2003). Here, we observed that neural trajectories corresponding to different VOCs traced different paths in the principal component space, validating that the identity of each lung cancer VOC was uniquely encoded by the honeybee ALN population responses.

2.2. Odor-evoked spatiotemporal antennal lobe neuron responses can be leveraged to identify lung cancer biomarkers

We then attempted to quantify the ability of the honeybee ALNs to classify cancer biomarkers by implementing a high-dimensional, leave-one-trial-out (LOTO) analysis scheme (Fig. 2a–f, see Experimental Section). First, a high-dimensional population response matrix was constructed as described before (Fig. 2a and b). Then, one trial was separated from the neural response matrices for each odor and used as a 'testing template' while the remaining four trials were averaged together and used to create the 'training templates' (Fig. 2c). This resulted in 10 training and 10 testing templates corresponding to nine lung cancer VOCs and the mineral oil control. Time-matched responses within a 50 ms bin of the training and testing templates were plotted in the high dimensional space and the Euclidean distances between each testing template and all 10 training templates were calculated. Testing templates were classified as belonging to the odor whose training template minimized a distance metric (Fig. 2d). This LOTO analysis was performed in such a way that each trial (out of the total five trials corresponding to one VOC) becomes the testing template once. Similar to trajectory analysis, this high-dimensional classification was also performed within the 0.25–0.75 s post-stimulus onset window. The results are summarized in a confusion matrix (Fig. 2e–g), with the testing templates along the X-axis and the training templates along the Y-axis. The higher classification success rates along the diagonal, shown by the darker colors, were indicative of testing templates being classified to the correct training template, resulting in an overall 50% success rate using a Euclidean distance metric. We would expect that a completely random assignment of odors would only yield 10% accurate classification in this case. This classification rate reflects how many of the 50 ms population response vectors can be classified correctly. To convert that number to classification success over the entire 500 ms discriminatory neural response window, we took the mode of the 50 ms bin-wise classification values over the duration of each 500 ms trial in a winner-take-all manner (Fig. 2f–h). Using this method with a Euclidean distance metric, we achieved 88% classification success of all cancer biomarkers tested.

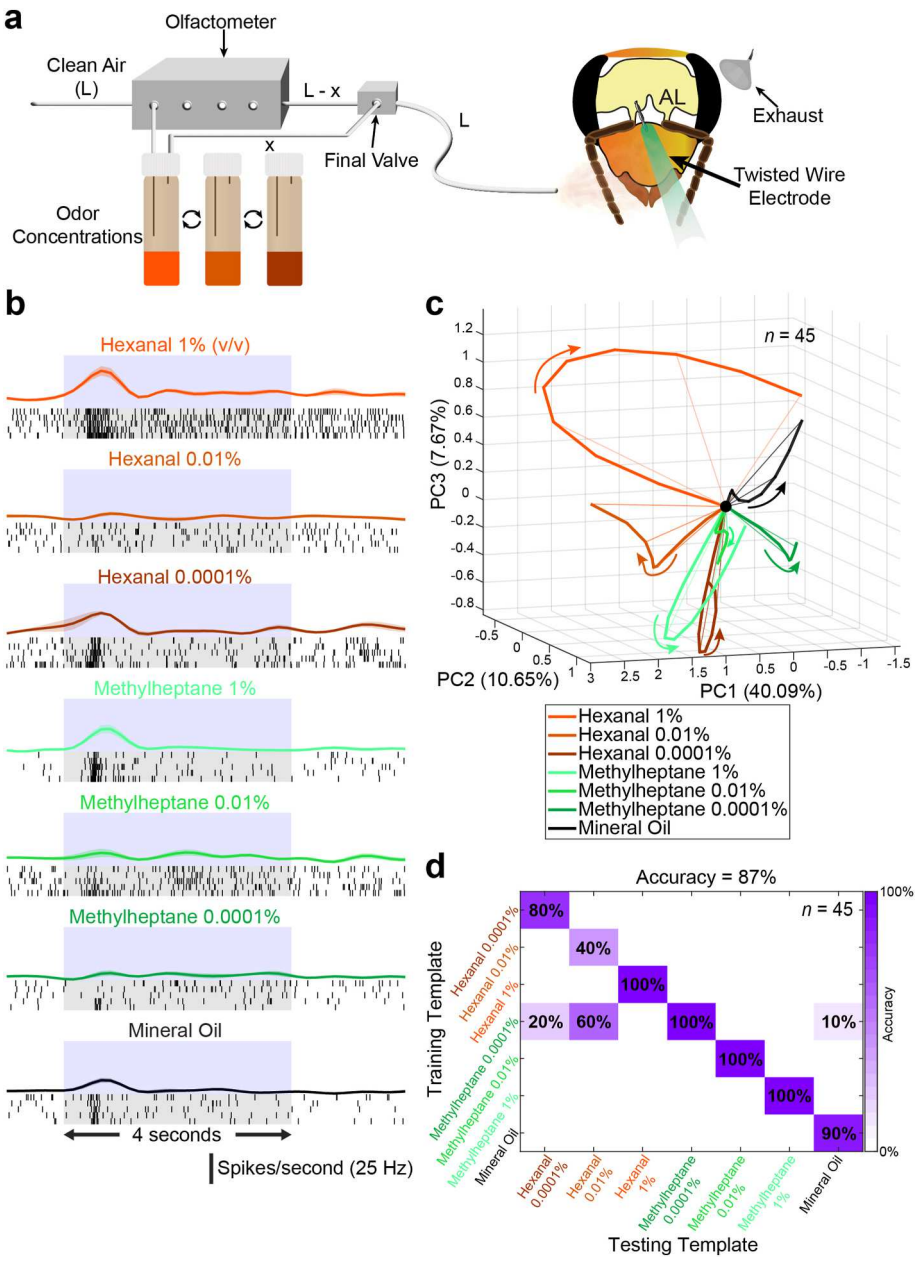

Fig. 3. Varying concentrations of lung cancer biomarkers can be classified by population neural responses. (a) Schematic of experimental setup. Single VOCs mixed with mineral oil at three concentrations (1% v/v, 0.01% v/v, 0.0001% v/v) are delivered to the honeybee antennae. **(b)** VOC-evoked voltage responses shown in Supplementary Fig. 2 were spike-sorted. The peri-stimulus time histograms (PSTHs) and raster plots of one antennal lobe neuron's responses to all 7 odors and concentrations are shown. Raster plots are shown for all five trials of each VOC (4 s duration of odor presentation). Note the reliability of spiking responses over trials separated by 60 s inter-stimulus interval. Trial-averaged PSTHs showing the spiking rate over time are plotted with the shaded region indicating the SEM. The light blue and grey box indicate the 4-s odor presentation window. **(c)** VOC-evoked population neural trajectories of all 7 odors are shown using PCA dimensionality reduction. The trajectories are plotted between 0.25 and 0.75 s after stimulus onset. The colored arrows indicate the direction of evolution for each VOC-evoked trajectory. All trajectories are aligned at 0.25 s after odor onset (indicated by a black dot), which corresponds to the time of the odor plume hitting the antennae after the opening of the final valve (at 0.0 s). **(d)** Using the high dimensional leave-one-trail-out (LOTO) analysis, the entire time window between 0.25 and 0.75 s after stimulus onset is classified with an accuracy of 87%. This indicates that the sensor can detect lung cancer biomarkers at different concentrations.

2.3. Lung cancer biomarkers can be detected at different concentrations employing the honeybee olfactory neural responses

To further explore the honeybee's capability of detecting cancer biomarkers, we tested varying concentrations of two biomarkers that elicited strong neural responses (Fig. 1, hexanal and 2-methylheptane). For each biomarker, we mixed three concentrations starting at the previously tested value of 1% vol/vol and decreasing towards biologically relevant concentrations (Fuchs et al., 2010; Poli et al., 2005) (0.01% vol/vol and 0.0001% vol/vol, diluted in mineral oil) (Fig. 3a) (see Experimental Section). Odor stimuli were presented to the honeybee antennae in a pseudorandom order using a procedure controlling for timing, delivery, and airflow (see Experimental Section).

For each biomarker concentration, we recorded odor-evoked responses from multiple ALNs (Supplementary Fig. 2b). Individual neuron responses were observed through raster plots and PSTHs (Fig. 3b, representative neuron). Interestingly, odor-evoked responses displayed clear differences between biomarkers and between different concentrations of the same odor. We employed the spike rate-based analysis described earlier with 50 ms time bins (Fig. 2a and b) to visualize and

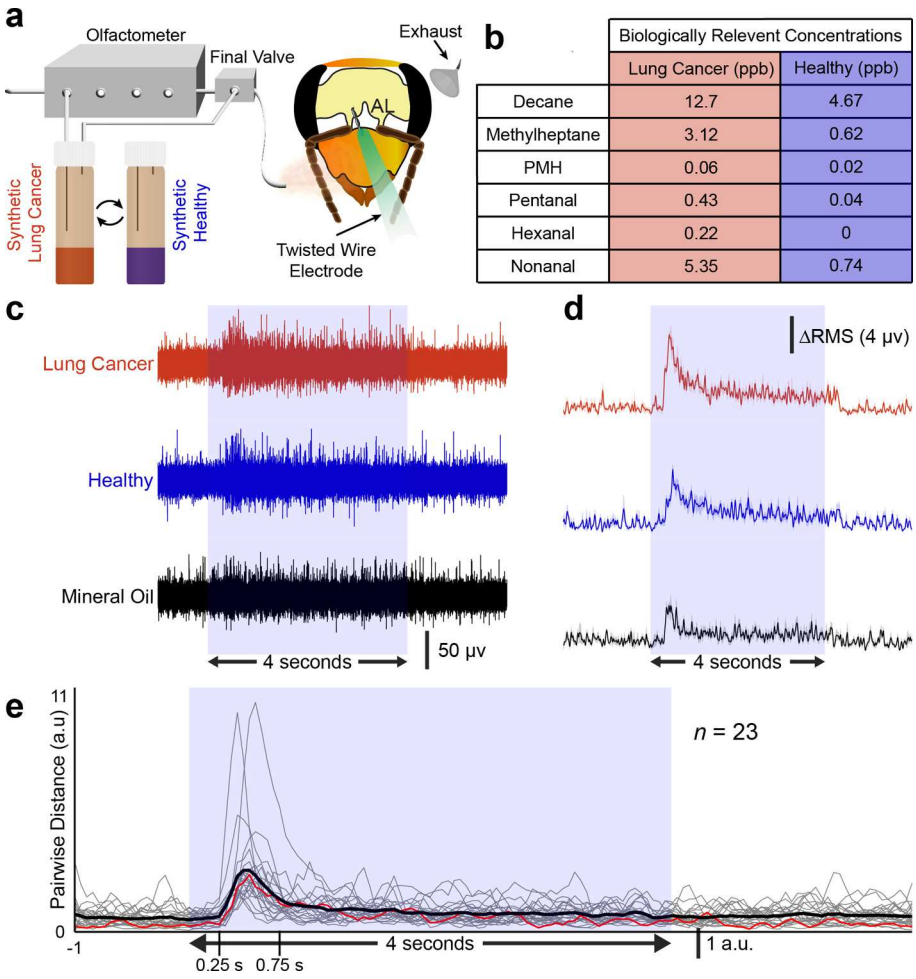

Fig. 4. Synthetic lung cancer vs. healthy breath mixtures can be distinguished by individual ALN recordings. (a) Schematic of the odor delivery and neural recording setup. Notice that instead of single VOCs being delivered, now a complex mixture of VOCs (synthetic lung cancer patient breath or synthetic healthy patient breath) is delivered to the honeybee antennae. **(b)** Table of concentrations for the six VOCs mixed into the two synthetic breath mixtures. These concentrations are derived from GC-MS studies (Lim et al., 2018; Chen et al., 2015). **(c)** Neural voltage responses of a representative ALN recording are shown for synthetic lung cancer breath, synthetic healthy breath, and mineral oil control. Notice that even at ppb level concentrations of the VOC mixtures, the neural recordings show clear odor-evoked responses during the odor presentation window. **(d)** R.M.S. filtering has been applied to the voltage traces and averaged across the four channels of the twisted wire electrode. The increase in voltage after stimulus onset followed by a slightly above baseline voltage for the remainder of the stimulus preserves the response patterns observed in the voltage traces in **panel c**. **(e)** Pairwise distance plots are shown using the same method as in Fig. 1d. Here, 23 R.M.S. voltage traces are plotted (grey). The red line indicates the pairwise distances for the R.M.S. trace shown in **panel d** and the black line is the average of all 23 R.M.S. voltage traces. Again, notice that the maximum pairwise distances for most positions is between 0.25 and 0.75 s after stimulus onset.

classify odor-evoked population neural responses. A population PSTH of change in firing rate for every odor was created by averaging the spikes of all neurons ($n = 45$ ALNs) in each time bin (Supplementary Fig. 2a). We observed the greatest change in firing rate occurred during 0.25–0.75 s after the odor onset and chose this time window for data analyses.

By plotting the population neural trajectories of each odor concentration (PCA, see Experimental Section), we observed clear separation between biomarkers and concentrations (Fig. 3c). These results showed that although the odor chemical is the same, the honeybee antennal lobe neurons recognized the change in concentration effectively resulting in a different encoding of information. Additionally, we used a second dimensionality reduction technique, linear discriminant analysis (LDA) (see Experimental Section), which is a supervised algorithm that maximizes between-cluster separation while minimizing within-cluster variance. We saw that all seven odors created separate clusters within the space suggesting satisfactory differentiation for classification (Supplementary Fig. 2c).

Quantitative analysis of classification success rate between the two cancer biomarkers and their varying concentrations was performed using a high-dimensional LOTO analysis (see Experimental Section, Manhattan distance used). For trial-wise classification across the entire time window (0.25–0.75 s), the success reached 87% (Fig. 3d). The honeybee antennal lobe was able to discriminate between all three concentrations of 2-methylheptane at a success rate of 100% whereas the classification rate was lower for different concentrations of hexanal (Fig. 3d). These results demonstrated that honeybees could distinguish between multiple lung cancer biomarkers at very low concentrations (e.g., 0.0001 vol/vol).

2.4. Synthetic human lung cancer breath vs. synthetic healthy breath can be differentiated by the honeybee antennal lobe neuronal responses

After verifying that several human lung cancer biomarkers can be detected by the honeybee ALNs at different concentrations (Figs. 1–3), we tested if complex mixtures that replicate actual concentrations of these VOCs in the exhaled breath of healthy individuals vs. lung cancer patients can be detected by the honeybee ALN responses. We defined these complex VOC mixtures as 'Synthetic breath' mixtures (Fig. 4a). We leveraged previously published concentration data of the VOCs (Fuchs

et al., 2010; Poli et al., 2005), combined six VOCs at specific concentrations as found in lung cancer vs. healthy human exhaled breath samples, and mixed them in clean air (80% nitrogen and 20% oxygen) to reach the desired biological concentrations at ppb to ppt ranges (Fig. 4b).

Even at these low VOC concentration mixtures, we observed clear odor-evoked responses from the ALNs to the synthetic breath stimuli (Fig. 4c and d). Instead of employing a spike rate-based analysis, the data was processed using a root mean squared (R.M.S.) transform-based approach, which can be implemented automatically and in real-time (see Experimental Section). The R.M.S. transform preserves the overall shape of the voltage trace as shown in our previous work (Farnum et al., 2023). For example, at a representative position shown in Fig. 4d, the synthetic lung cancer breath elicited the largest peak in the R.M.S

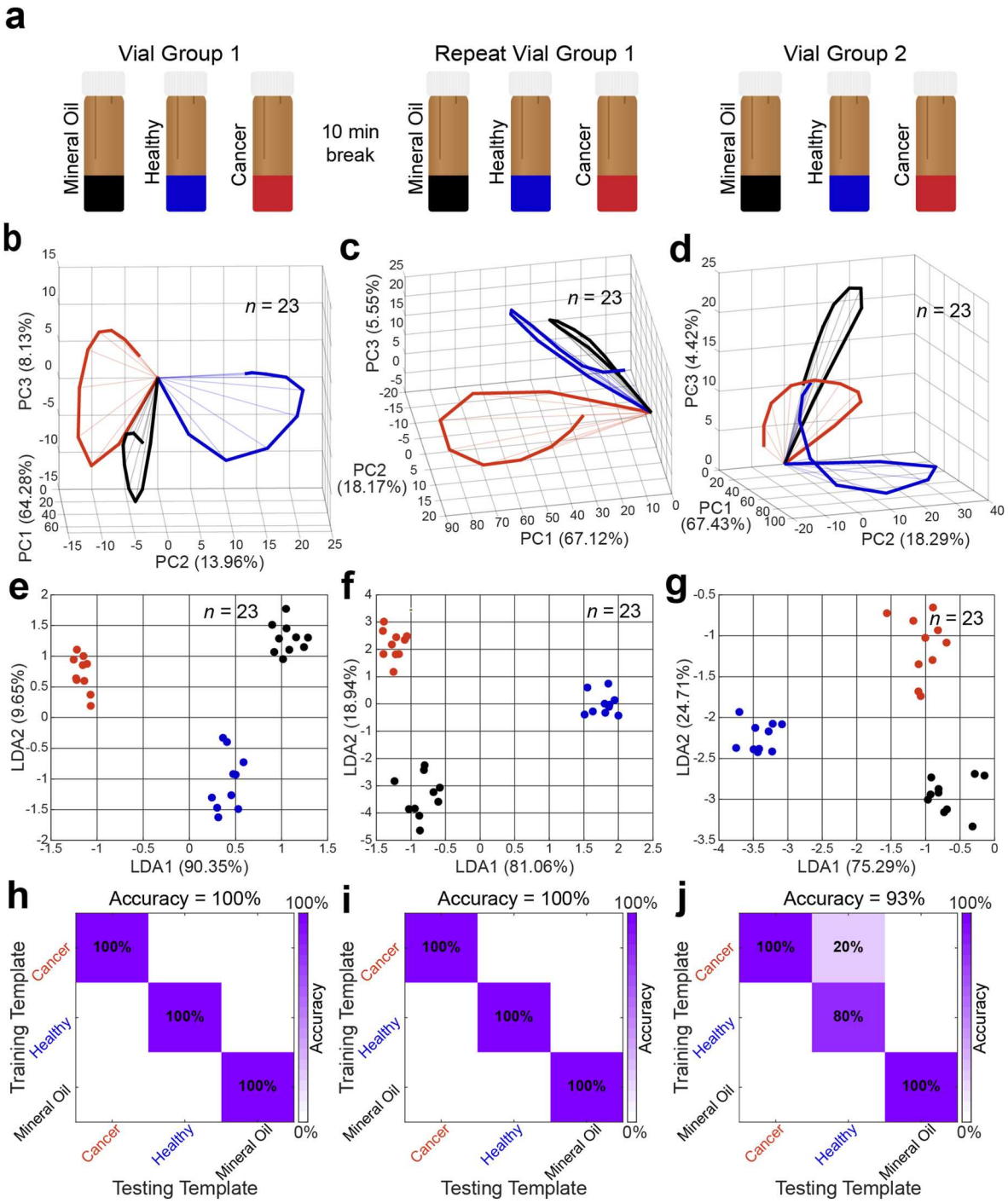

Fig. 5. Population analysis of the synthetic breath mixtures shows reproducibility across multiple odor panels. (a) The population neural responses shown in columns one and two are both elicited from the exact same odor vials with a 10-min time interval between stimulus presentations. Here, if we imagine the honeybee as a sensor, the two columns are akin to technical or analytical replicates. Population neural responses shown in column three are elicited from a different set of odor vials that were produced using the exact same procedure as the first set of vials. Again, if the honeybee is a sensor, this is akin to a sample replicate. **(b–d)** PCA trajectories of the 23 R.M.S. voltage traces of the three odors all project in different directions for each panel. **(e–g)** 3-class LDA, a supervised dimensionality reduction technique, clearly separates the odors into three distinct clusters. **(h–j)** LOTO analysis of the entire transient response period (0.25–0.75 s after stimulus onset), as described for Fig. 2h, correctly classifies every trial except one in Fig. 5j.

transformed odor-evoked response while the mineral oil control elicited the smallest peak.

Next, to confirm that the recording sites contain discriminatory information corresponding to synthetic lung cancer vs. healthy breath mixtures, a pairwise distance analysis, previously used for the spike-sorted individual cancer biomarker-evoked responses, was implemented for the R.M.S transformed synthetic breath responses. Again, most of the recorded positions showed differences in the neural responses to the synthetic lung cancer vs. healthy breath, with the largest difference between the responses occurring during the transient odor response window from 0.25 to 0.75 s (Fig. 4e).

2.5. Honeybee population neural responses classify synthetic lung cancer vs. healthy breath reliably and at a high success rate

How precisely and repeatably can lung cancer vs. healthy breath mixtures be classified at the population ALN level? To address this question, we performed an experiment where synthetic lung cancer vs. healthy breath mixtures were delivered repeatably to the honeybee brain. To test the reproducibility of the classification performance, the odor samples were varied in two different manners: (1) same odor mixtures (from the same odor bottle) were temporally separated by a 10-min gap between presentations, and (2) same odor mixtures were delivered from a different set of odor bottles that were mixed separately, following the same protocol (Fig. 5a). This was done to incorporate any variations due to the serial mixing of VOCs at low concentrations. The first set of results of synthetic lung cancer vs. healthy odor mixture are shown in Fig. 5b–e,h, the 10-min delayed repeated odor presentation data is shown in Fig. 5c–f,i, and the results for the odor presentation from different bottles are shown in Fig. 5d–g,j. To observe the mixture classification results, population neuronal trajectories were plotted corresponding to synthetic lung cancer vs. healthy breath mixtures (see Experimental Section). Briefly, R.M.S. transformed neural responses were binned into discrete 50 ms bins by averaging the voltage values within each bin and subsequently converted into odor-specific population matrices, using the same procedure as previously implemented on individual cancer biomarker data (Fig. 1e and 3c). Within the PCA subspace, all three odors (synthetic lung cancer breath mixture, synthetic healthy breath mixture, and mineral oil control) were clearly projecting in different directions away from the origin demonstrating good separation between the neural responses to all three stimuli (Fig. 5b–d). This result indicates that although only small variations in concentrations (i.e., ppt level) exist between healthy vs. lung cancer synthetic breath mixtures, they are encoded differently by the neuronal population in the honeybee antennal lobe, which can be leveraged to classify those mixtures using population neuronal response templates. These results were similar when we analyzed the data collected after a 10-min break (Fig. 5c) and from a different set of bottles (Fig. 5d) indicating the repeatability of our population response trajectory results.

Next, we tested how well the lung cancer vs. healthy breath mixture-evoked neuronal responses are separated using a second technique, LDA. We observed that the three odors formed separate, distinct, and cohesive clusters (Fig. 5e–g) indicating good separation between them for all three different stimulus delivery conditions.

Finally, to quantify the classification success rates of lung cancer vs. healthy breath mixtures, we employed a high dimensional LOTO analysis (see Experimental Section). When we looked at the classification success across the entire 0.25–0.75 s time window, which we already established as the most discriminatory part of the neural signal, the classification success reached 100% using the LOTO approach (Fig. 5h). We performed the same analysis using spike sorted ALN data on the synthetic breath mixtures and obtained similar classification results (Supplementary Fig. 3). We observed comparable classification success results for temporally separated synthetic breath samples (Fig. 5i) and the samples from separately mixed bottles (Fig. 5j).

2.6. Honeybee brain olfactory neurons can detect VOCs from human lung cancer cell lines using the 'smell' of cultured cell lines

Finally, we sought to explore the capabilities of our sensor for the detection of VOCs produced from cultures of human lung cancer cell lines. To achieve this, we cultured six different human lung cancer cell lines and a healthy lung fibroblast cell line (see Experimental Section). Briefly, cell lines were cultured for four days before being split and resuspended in modified sterile T-25 flasks the day prior to experimentation. Additionally, a flask containing the same media used to resuspend all other cell lines was created as a control. Out of the six lung cancer lines chosen, four were NSCLC (NCI–H1975, NCI–H661, NCI–H1437 stage 1, NCI–H1573 stage 4) and two were SCLC (SHP-77, H69PR). This selection of cell lines allowed us to test the discrimination ability of our sensor between lung cancer vs. healthy cells, the two main lung cancer cell types (NSCLC vs. SCLC), as well as the cancer sub-types (different cell lines, adenocarcinomas and carcinomas, of the same main type). Cell flask caps were tightened 1–2 h before experimentation to trap VOCs and then microscopic images were taken to ensure that all the cell lines were healthy. Representative images of all cell lines including the media flask are presented in Supplementary Fig. 4. During experimentation, cell culture flasks were kept incubated at 37 °C and only removed when needed for odor presentation (~5 min at room temperature). Cell culture flasks were attached to the olfactometer through odor lines and presented to the honeybee antennae in a pseudorandom order (Fig. 6a).

Distinct odor-evoked responses were observed for each cell line with multiple neurons firing in the brain tissue. A representative voltage trace recording is shown in Supplementary Fig. 5b. PSTHs and raster plots were used to visualize individual neuron responses to cell lines. Neurons were collected after spike sorting each odor-evoked multiunit voltage trace (see Experimental Section). Clear differences in firing rate between healthy cells, cancer cells, and media control were seen at the individual neuron level, a representative neuron is shown in Fig. 6b. A population PSTH of firing rate from all the neurons collected showed that the greatest variability of odor-evoked response happened between 0.25 and 0.75 s after odor stimulation (Supplementary Fig. 5a). This time window was used in classification analyses moving forward.

To further investigate differences in olfactory responses between healthy and lung cancer cell lines, odor-evoked population neural trajectories were plotted using a PCA dimensionality reduction technique (see Experimental Section). Neural trajectories of each cell line followed separate paths through the PCA space, displaying clear distinctions between healthy, NSCLC, SCLC, and media control (Fig. 6c). A second dimensionality reduction technique, LDA, visualized population neuron clusters for each cell line. Though not as clear as the PCA, we still observe some odor clustering in the center of the LDA space which gets more distinct as you move outwards (Supplementary Fig. 5c). These dimensionality reduction techniques show that the honeybee olfactory system possesses a unique coding mechanism for different lung cell line types (healthy, NSCLC, SCLC).

Finally, a high-dimensional LOTO analysis was used to classify the human lung cancer detection success rate of the honeybee olfactory system (see Experimental Section, Manhattan distance used). We looked at the classification accuracy for healthy human lung cells vs. NSCLC vs. SCLC and found that the honeybee was able to classify all cell lines with 82% accuracy (Fig. 6d). The vast majority of cell lines had a very high classification accuracy with media and two NSCLC lines (NCI–H1975 and NCI–H1437–S1) achieving 100%, one NSCLC (NCI–H661) and SCLC (H69PR) cancer line being 90%, healthy human lung fibroblasts (HLF) reaching 80%, and the second SCLC (SHP-77) cancer line being 70%. The sensor classified one NSCLC cell line (NCI–H1573–S4) 27% correctly, which was low compared to the other cell lines tested. Overall, these results demonstrate that the honeybee olfactory system is capable of identifying the complex VOC mixture differences produced by different cell types, uniquely encoding that olfactory information, and

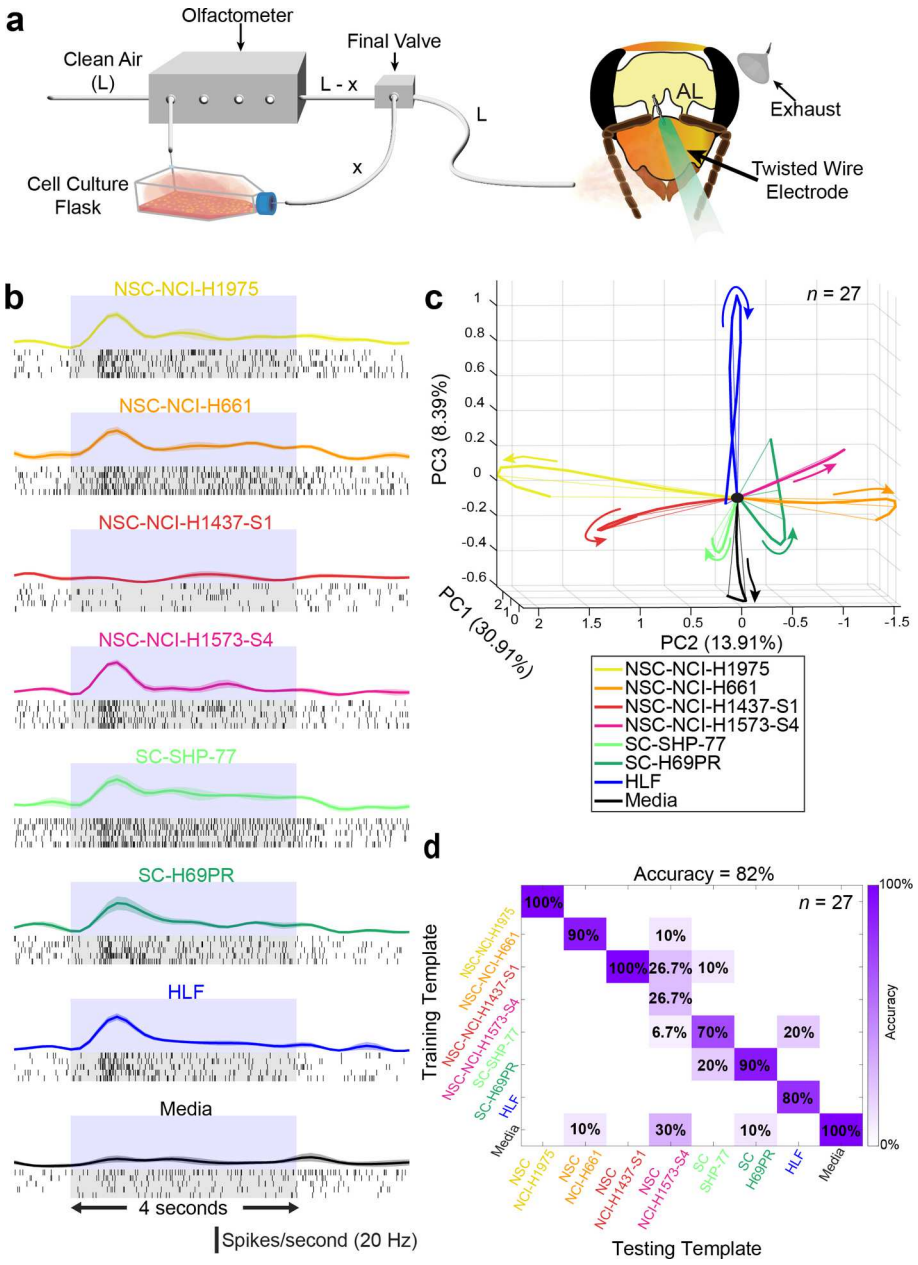

Fig. 6. Human lung cancer cell lines can be classified and distinguished from one another using the brain-based sensor. **(a)** Schematic of the experimental setup. VOC mixtures emitted from human lung cancer cell lines were delivered to the honeybee antennae using cell culture flasks. During experimentation, flasks were kept in an incubator at 37 °C and were taken out one at a time only for odor presentation. Four NSCLC cell lines, two SCLC cell lines, one healthy lung cell line, and the media control were chosen for this experiment. Representative cell culture images are shown in Supplementary Fig. 4. **(b)** Cell culture-evoked voltage responses shown in Supplementary Fig. 5 were spike-sorted. The peri-stimulus time histograms (PSTHs) and raster of one antennal lobe neuron's responses to all 8 odors are shown. Raster plots are shown for all five trials of each cell culture presentation with each black line indicating a spike from the neuron. Trial-averaged PSTHs showing the spiking rate over time are plotted with the shaded region indicating the SEM. The light blue and grey box indicate the 4-s odor presentation window. **(c)** Cell culture VOC-evoked population neural trajectories of all 8 odors are shown using PCA dimensionality reduction. The trajectories are plotted between 0.25 and 0.75 s after stimulus onset. The colored arrows indicate the direction of evolution for each cell culture-evoked trajectory. All trajectories are aligned at 0.25 s after odor onset (indicated by a black dot), which corresponds to the time of the odor plume hitting the antennae after the opening of the final valve (at 0.0 s). **(d)** High dimensional LOTO analysis of the transient response period (0.25–0.75 s after stimulus onset) classifies with an accuracy of 82%.

correctly classifying it against media control, healthy cells, distinct types of lung cancer (NSCLC and SCLC), and most impressively, between different cell lines of the same type of lung cancer.

3. Discussion

Early detection of cancer with tools that are rapid, available and sensitive is essential to improve patient outcomes by allowing for a greater chance of successful treatment, and therefore a higher likelihood for recovery. The current recommended technology for lung cancer screening is a radiation imaging technique called low-dose commuted tomography (LDCT) (Oudkerk et al., 2021). Using this method to screen high-risk patients has improved overall lung cancer mortality, but this technique is not readily available to everyone, has known issues with false positives, and the associated risks due to exposure to ionizing radiation prohibit use for screening in the general population (Baldwin and Callister, 2016).

Specific biomarker detection (e.g., DNA, RNA, or proteins) from

body fluids using advances in material science have shown promising results for the early detection of many diseases, including viral infections and cancers (Iqbal et al., 2022; Panicker et al., 2023). Human epidermal growth factor receptor 2 (HER2)–positive breast cancer is a prime example of targeted detection and therapy, in which a single molecule has enabled a radical shift in cancer treatment. However, HER2-positive breast cancer only accounts for 20% of all breast cancers (Kunte et al., 2020) and while HER2 is specific to a single type of cancer, most biomarkers have been generally associated with many different cancers (e.g., microRNA-150, a specific microRNA sequence, is associated with colorectal, gastric, leukemia, and lung cancer) (Iqbal et al., 2022; Haick et al., 2014). This lack of specificity for many cancer biomarkers can make diagnoses and treatment difficult. While specific biomarker detection can be incredibly sensitive, it is limited by the heterogenous nature of cancer.

Breath-based diagnostics offers a promising alternative cancer screening modality due to its inherent noninvasiveness and the possibility for reliable and early detection based on distinct metabolic differences. The human body emits a variety of VOCs that are released from breath, sweat, urine, feces, and vaginal secretions (Shirasu and Touhara, 2011). Several factors such as diseases (Nardi-Agmon and Peled, 2017; Gruber et al., 2014; Lim et al., 2014; Mochalski et al., 2018; Phillips et al., 2020), exercise, food consumption, and drug use (Amann et al., 2014) are known to alter the components and concentrations of VOCs, and thus can reflect the metabolic condition, or health, of an individual. A wide variety of VOCs at specific concentrations have been associated with cancer (Haick et al., 2014) from multiple *in vitro* and *in vivo* studies spanning lung (Jia et al., 2018; Thriumani et al., 2018; Davies et al., 2014; Peled et al., 2013; Janssens et al., 2022; Serasanambati et al., 2019b), breast (Lavra et al., 2015), leukemia (Tang et al., 2017), gastric (Xu et al., 2013), and prostate cancer (Lima et al., 2018). Different chemical compounds including hexanal, propanal, pentanal, acetone, pentane, 2-butanone, and benzene at specific concentrations have been identified as potential lung cancer biomarkers (Jia et al., 2019). Overall, there is growing evidence that VOCs in the breath of cancer patients are altered compared to healthy individuals (Gower et al., 2023; Binson and Subramoniam, 2022; Ratiu et al., 2020; Xiang et al., 2021), and these unique compositions of VOCs in exhaled human breath can be used as a fingerprint for the early detection of cancer. We have shown that honeybees can detect all nine of the different lung cancer associated VOCs we tested, indicating their capacity to be a breath-based diagnostic sensor.

E-noses are portable sensors that implement biological principles of gas sensing to achieve one-shot complex VOC mixture classification. They detect and quantify VOCs in a breath sample by converting the interaction of VOCs with different materials into electrical signals, which are then processed using cross-selective sensors and template-matching analyses (Baldini et al., 2020; Röck et al., 2008; Ko and Park, 2016). These e-nose devices have also been used to effectively classify multiple types of cancers, including lung (VA et al., 2021; van Geffen et al., 2019), prostate (Filianoti et al., 2022), and head and neck (Anzivino et al., 2022). E-noses are simpler and more portable than GC-MS, making them suitable for point-of-care and home-based VOC analysis. However, e-noses have a lower specificity and sensitivity compared to GC-MS and are generally not able to detect all the VOCs in a breath sample, especially at low concentrations (Hurot et al., 2020; Röck et al., 2008). Some e-noses have recently started incorporating biological olfactory receptors and live cells for VOC sensing (Lim et al., 2014; Cave et al., 2019; Lu et al., 2014; Wu, 1999; Yang et al., 2017; Jin et al., 2012; Vidic et al., 2007; Ahn et al., 2015; Sankaran et al., 2011; Larisika et al., 2015; Misawa et al., 2010). However, using only one or few biological receptors does not provide robust detection capabilities for these e-noses and their reliability of detection over time remains an issue. Using the broadly sensitive honeybee olfactory sensory system, with no need to know or design the sensor for specific VOC identity or concentration ranges, we reliably classified all nine potential lung cancer biomarkers, synthetic breath mixtures, and six human lung cancer cell lines.

Biological olfaction, such as a dog's nose, has been used to detect several types of cancer, including lung cancer, from human breath samples (Cornu et al., 2011; Urbanová et al., 2015; Pickel et al., 2004; Willis et al., 2004b; Gordon et al., 2008; Horvath et al., 2011; Ehmann et al., 2012; McCulloch et al., 2006; Lee et al., 2015). Similar to dogs, more recently, behavioral studies involving other animals including rats, honeybees, fruit flies, and ants have been conducted to detect different diseases (Lee et al., 2015; Mgode et al., 2012; Weetjens et al., 2009; Kontos et al., 2022; Suckling and Sagar, 2011; Strauch et al., 2014; Piqueret et al., 2022). However, behavioral studies are susceptible to behavioral variations due to other sensory cues and result in binary outcomes - 'yes' or 'no,' which limits this approach to detect only one disease. Our approach eliminates behavioral variability by directly recording the cancer VOC-evoked neural signals from the honeybee's olfactory brain, which is known to be odor identity and intensity specific and can detect odor stimuli in natural environments (Stopfer et al., 1997, 2003; Saha et al., 2013a, 2013b, 2015, 2017, 2020; Raman et al., 2010; Stopfer, 2014). Also, insect antennae are extremely sensitive, with a recent study indicating the detection threshold is sub-ppb (Neta et al., 2023). Therefore, we expect this honeybee brain-based odor detection approach will be robust, sensitive to the minute VOC concentrations in human breath, and work efficiently in natural settings.

Our previous work demonstrates that neural recordings from the locust brain can be employed to successfully differentiate between three types of human oral cancer cell lines from a human noncancer cell line (Farnum et al., 2023). However, in this previous work, we could not determine which VOCs were different between the oral cancer vs. noncancer cell lines as this biological neural template-based odor classification approach does not identify individual compounds. Therefore, here, we reverse-engineered the mixture of specific lung cancer VOCs that have been identified and shown to be different between lung cancer vs. healthy human breath samples through GC-MS based studies. We mixed those VOCs at precise concentrations to generate synthetic lung cancer and healthy breath mixtures. By using this synthetic breath approach, we were able to show that these different mixtures of six lung cancer associated VOCs can be successfully differentiated by honeybee olfactory neural recordings. Ours is the first study to confirm that mixtures of multiple volatile lung cancer biomarkers, at ppb to ppt levels, that mimic concentrations in exhaled human breath can be detected by honeybee olfactory neural circuitry. This study opens the door for employing powerful honeybee olfactory neural responses for noninvasive cancer detection.

This honeybee sensor is by no means limited to the detection of individual biomarkers or synthetic breath mixtures. We have demonstrated this broad sensitivity through the detection of human lung cancer cell lines. VOC-laden air from the headspace of these cell cultures was delivered to the honeybee antenna while concurrently recording neural responses from antennal lobe neurons for real-time detection. These neural responses to the naturally complex cell culture headspace VOCs create unique templates for classification. The honeybee olfactory system can distinguish between the healthy cell line, media control, and the two main types of lung cancer (NSCLC and SCLC). Our results stem from the detection of metabolic alterations characteristic of cancer leading to altered VOC profiles (Bamji-Stocke et al., 2018; Sertorio et al., 2018; Zhou et al., 2012). Evidence has shown that metabolites relating to lipid metabolism and cellular growth have a significant increase in concentration in lung cancer compared to healthy cells as the cancerous cells switch from glycolysis to oxidative phosphorylation for energy production, changing the emitted VOCs (Puchades-Carrasco et al., 2016; Eigenbrodt et al., 1998; Pereira et al., 2015b). For lung cancer, NSCLC and SCLC have unique metabolic and morphologic characteristics compared to normal, healthy cells (Lim et al., 2018; Pedersen et al., 2021; Sertorio et al., 2018). There are many differences relating to cell morphology (Lim et al., 2018; Puchades-Carrasco et al., 2016), growth

rate (Lim et al., 2018; Puchades-Carrasco et al., 2016), and metabolism (Lim et al., 2018; Pisters et al., 1993; Maeda et al., 2010) between NSCLC and SCLC which contribute to slight differences in emitted VOCs that the honeybee is able to detect and differentiate. Based on our data, NSCLC can be accurately distinguished from SCLC by the honeybee olfactory system, with very little confusion between the cell lines of the same type of cancer. The cancer cell lines used for experimentation were chosen randomly without bias of the metabolic or morphologic diversity between lines. This aligns more with what one would find in a real-world application; however, any lack of diversity between cell lines could contribute to the classification confusion seen in some of the results.

Additionally, while our honeybee olfactory sensor successfully classified most lung cancer cell lines, it struggled with distinguishing NSC-NCI-H1573-S4 from others. Interestingly, in our study, this cell line was the only one chosen from American Type Culture Collection that was officially labeled as stage 4 lung cancer. It is known that as cancer progresses, the genetic diversity of the disease increases, thus allowing a wide range of genomic mutations that coexist (Goto et al., 2018; Gentric et al., 2017; Dagogo-Jack and Shaw, 2018). This range of coexisting mutations are the basis of cancer heterogeneity as the disease advances, creating an immunocompromised microenvironment that tolerates change (Dagogo-Jack and Shaw, 2018). Lung cancer epitomizes changing over time by maintaining a significant increase in mutational burden, augmenting its heterogeneity with progression (Puchades-Carrasco et al., 2016; Pisters et al., 1993; Goto et al., 2018). This leads to various metabolic profiles and varied VOCs emitted as a consequence of increasing versatility and diversity (Dagogo-Jack and Shaw, 2018; Mendes et al., 2023). An increase in volatile profile heterogeneity could allow the odor to be increasingly challenging to differentiate, leading to the classification confusion seen within the results. Moreover, not all cell lines used in this study were specifically labeled with cancer stages, therefore additional exploration of late-stage cancer classification using our biological sensor should be done. Nonetheless, our study is the first to successfully employ a biological honeybee sensor in the detection of human lung cancer cells.

Reproducibility of the honeybee brain-based sensor's responses are evident from multiple observations: 1) each neuron's response to stimuli, 2) the population neural response to stimuli, and 3) the classification performance across replicates of the same stimuli. In each of our experiments, neurons exhibited similar responses to the same stimulus throughout five consecutive presentation trials (Fig. 1c, 3b and 6b). Therefore, the individual neurons we recorded from the honeybee AL were reproducibly responding to stimuli. The reproducibility of the population neural response to stimuli was measured by the high dimensional LOTO analysis, where the training template was based on four trials and the testing template was the left-out trial. As we achieved a high classification success rate for all different types of stimuli tested (single biomarkers, concentration gradients, VOC mixtures, and cell culture headspace VOC mixtures), it demonstrates that population neural responses are reproducible for each stimulus over multiple trials (Fig. 2h, 3d and 5h,i,j, 6d). Finally, we have demonstrated the reproducibility of the sensor's classification performance using temporally distinct delivery of the same odor mixture (technical replicate) and delivery from two different odor bottles mixed using the same procedure (sample replicate) (Fig. 5h,i,j). Notice that population neural responses, which are generated by combining neuronal responses across multiple honeybees, determine the classification performance of the sensor. Therefore, reproducibility of the sensor based on individual bees cannot be computed unless all the neurons are recorded from the same bee. However, in our future work, we plan to record large numbers of neurons from each honeybee, which will help determine reproducibility of the sensor based on individual bees.

The number of neurons recorded for each experiment can be increased by improving the multi-electrode configuration or by adjusting the placements of the electrodes within the antennal lobe. In the future, we expect to collect ~20–30 ALNs from one single honeybee, which would enable spatiotemporal classification of odors. The principles for achieving reproducibility between different honeybee brain-based sensors will depend on the generation of 'distinct' neuronal response templates corresponding to the target VOC mixtures (e.g., lung cancer vs. noncancer) and not on the identity of individual neurons. As we perform VOC-evoked extracellular neuronal recordings from the honeybee antennal lobe we expect that we will not be recording from the same neurons across different brains. Here, we have recorded from both PNs and LNs. The antennal lobe contains a dense interconnected network of roughly 800 PNs and 4000 LNs, both of which contain discriminatory odor information (Fonta et al., 1993; Paoli and Galizia, 2021). In this brain-based VOC sensing approach, the identity of individual neurons is not important, rather the properties of the entire recorded ALN population responses are the key. Our high dimensional template-based analysis replicates biological olfaction which transfers odor identity to higher-order brain centers based on the integrated and combined neural response within the antennal lobe. Also, just like biological systems, we do not specifically detect individual VOCs within a mixture, instead the response templates are based on the entire mixture, which is classified as a single odor. Our goal will be to create VOC-evoked ALN population response templates that are distinct for different odors in the neural response space from a single honeybee.

To show that honeybees can detect lung cancer through breath-based analysis, we have used complex gas mixtures of six compounds at ppb to ppt levels and mixed them with clean air to replicate lung cancer and healthy human breath. However, the exact concentrations of the hundreds of VOCs in the breath of lung cancer patients and healthy individuals are unknown and therefore we cannot synthetically replicate the concentrations of all the VOCs present in actual human breath. While cell cultures of different cancer cell lines will have subtle differences in VOC concentrations and exhibit many of the same VOC identities as exhaled breath, they will not perfectly replicate the VOCs that will be found in exhaled breath. Finally, for each analysis, we used known odors to create neural response templates for single VOCs, concentration gradients of single VOCs, complex mixtures of VOCs, and healthy and cancerous cell lines. In the next stage, this honeybee olfactory neural circuit-based VOC sensing approach needs to be tested on human breath samples of lung cancer patients and healthy subjects.

Despite the honeybee brain-based sensor's lifetime being limited (~2–3 h), it is capable of running a new VOC test every minute (i.e., high throughput). In the future, this sensor can be applied to screen breath samples of several at-risk individuals (~40–50 patients) participating in a lung cancer clinic. For these sets of experiments, exhaled breath samples of patients will be collected in sorbent tubes, stored at −85 °C, and transported to the biosensing lab within 30 days of collection. Breath samples will be thermally desorbed and then the VOC mixtures will be delivered to the honeybee brain-based sensor using an olfactometer (following the same procedure used in these experiments). The sensor will be calibrated before testing unknown breath samples. During the calibration phase of the experiment, known breath samples (lung cancer vs. healthy breath) will be used to generate the training odor templates, which will be employed later to classify unknown breath samples based on the overlap between the lung cancer vs. healthy training templates with the exhaled breath testing template. Additionally, with a large and well-defined set of training breath samples, this sensor could be calibrated to distinguish between lung cancer subtypes of NSCLC and SCLC, as demonstrated in the experiments with cell lines.

4. Experimental Section

4.1. Honeybee husbandry

Foraging honeybees (*Apis mellifera)* were purchased and shipped from the School of Life Sciences at Arizona State University (Tempe campus, AZ, USA). The small colonies were maintained in an incubator in 24 h of darkness at 32 °C and 60% humidity for 4 weeks at a time. For

food, the bees were given 50% sucrose solution and pollen patties.

4.2. Honeybee surgery

The honeybees were collected individually into plastic vials, then placed briefly into ice. As soon as they stopped moving, the bees were manipulated into a plastic restraining harness with dental wax (Surgident Periphery Utility Wax) placed at the back of the head to prevent the head from moving while allowing free movement of the antennae and mouthparts. The bees were then left undisturbed on the counter for 30–60 min, after which they were fed 50% sucrose solution until they were completely satiated. The bees were then placed into a drawer overnight, along with a small cup of water for humidity. The next morning, the bees were tested for feeding motivation as a metric to determine their health for the electrophysiological recording. This was done by exposing the antennae to the 50% sucrose solution, and if a subsequent proboscis extension response was not observed, those bees were discarded. Eicosane wax (Sigma-Aldrich) was used to immobilize the antennae by first applying the wax to the base of the scapes and then to the pedicels, and then positioning the antennae so that the flagellum were both forward-facing. The top of the head was shaved using a microscalpel, and the bees rested undisturbed for 10–20 min. Next, a small window was cut into the top of the head just above the antennae and below the ocelli. The glands and tracheae were removed to expose the brain. The brain was kept hydrated with a Ringer's solution described by Brill et al. (in mM as follows: 37 NaCl, 2.7 KCl, 8 Na_2HPO_4, 1.4 KH_2PO_4; pH 7.2; all chemicals from Sigma-Aldrich)(Brill et al., 2013). The antennal lobe portion of the brain was desheathed just prior to electrode placement.

4.3. Odor vial preparation

For the individual cancer biomarkers, the following odorants were used: decane, undecane, 2-methylheptane, 2,2,4,6,6-pentamethylheptane (PMH), pentanal, hexanal, nonanal, propylbenzene, and trichloroethylene (all from Sigma-Aldrich). These odors were diluted in 10 mL of mineral oil at 1% vol/vol concentration, and the pure mineral oil was used as a control.

For varying concentrations of two chosen cancer biomarkers, hexanal and 2-methylheptane, we diluted both odors in 10 mL of mineral oil at 1% vol/vol and 0.01% vol/vol A serial dilution with the 1% vol/vol vials was used to generate the concentration of 0.0001% vol/vol in 10 mL of mineral oil.

To generate the synthetic lung cancer and healthy breath mixtures, we used the vapor pressure of each VOC and Raoult's Law to obtain the liquid phase volumes necessary to achieve the desired gas phase concentrations of each chemical compound that have been previously reported in the literature (Fig. 4b) (Fuchs et al., 2010; Poli et al., 2005). For the synthetic lung cancer breath mixture, the following odorants at their respective concentrations in the liquid phase were used (concentrations in μM): 1.0 pentanal, 1.1 hexanal, 390.9 nonanal, 240.0 decane, 15.2 2-methylheptane, and 0.8 PMH. For the healthy breath mixtures, the following concentrations were used (concentrations in μM): 0.1 pentanal, 0.0 hexanal, 54.1 nonanal, 88.2 decane, 3.0 2-methylheptane, and 0.3 PMH. Serial dilution was used to create these mixtures in 10 mL of mineral oil.

4.4. Cell culture preparation

T-25 flasks Nunc™ EasYFlask™ (Thermo Fisher Scientific, MA, USA) were modified in a sterilized cell culture hood prior to cell culturing. Using a handheld Dremel, 0.7 mm holes were drilled through the top of the flask near the back and through the cap of each flask. Inlet and outlet 20-gauge needles were inserted into each hole. The sharp end of the needles were sheered, and the base was stabilized using a low-volatile, two-part Permatex™ epoxy at least 24-hrs prior to seeding. The ends of the needles were capped with an air-tight epoxied tube to culture cell lines.

Six human lung cancer cell lines were purchased from American Type Culture Collection (ATCC) including three non-small adenocarcinoma cell lines: NCI–H1975 (derived from site: in situ; lung), NCI–H1437 [stage 1] (derived from site: metastatic; pleural effusion), NCI–H1573 [stage 4] (derived from site: in situ; lung), one non-small cell carcinoma cell line: NCI–H661 (derived from site: metastatic; lymph node), and two small cell carcinoma cell lines: H69PR (derived from site: metastatic; pleural effusion), SHP-77, non-adherent cells (derived from site: in situ; lung, left upper lobe). As a non-cancer control, primary lung fibroblasts, normal, human, HLF (derived from site: in situ, lung) were also purchased from ATCC. All cancer cell lines were seeded in surface treated sterile tissue culture flasks, vented cap, T75 at a density of 1.2×10^6 cells per flask in RPMI 1640 Medium with 10% heat-inactivated fetal bovine serum (FBS) and 1% penicillin-streptomycin (10,000 U/mL) at 37 °C in 5% CO_2 (T75 flasks, medium, FBS, and penicillin-streptomycin were all purchased from Thermo Fisher Scientific, MA, USA). The HLF line was cultured in Fibroblast Basal Medium (ATCC) with Fibroblast Growth Kit-Low serum (ATCC) at 37 °C in 5% CO_2 in the same T75 flasks. After 4 days, all adherent cells were detached using 4 mL of Accutase® solution (Sigma Aldrich) for 5 min, centrifuged at $160 \times g$ for 6 min, and the supernatant was then decanted. All cell lines were resuspended in 4 mL of RPMI complete medium at a seeding density of 2.25×10^6 cells per modified T-25 flasks. The cell lines and a RPMI complete media control were then incubated at 37 °C in 5% CO_2. Subsequently, the cells were subjected to olfactory testing.

4.5. Odor stimulation

Odor delivery was conducted following our pre-established methodology. Briefly, a commercial olfactometer (Aurora Scientific, 220A) was used for precision odor stimulus delivery (Fig. 1a). At the beginning of each set of trials, 200 standard cubic centimeters per minute (sccm) of zero contaminant air was passed through the fresh air flow line via a 1/16 in. diameter PTFE stimulus flow line to the honeybee antenna, and an additional 200 sccm of zero contaminant air was passed through the dilution flow line to the exhaust. The end of the stimulus flow line was positioned approximately 2–3 mm from and pointing at the most distal antennal segment. Five seconds prior to stimulus delivery, 40% (80 sccm) of the dilution line was redirected through the odor flow line directly upstream of the odorant vials or cell culture flasks. The dilution flow and odor line joined downstream of the odorant vials or cell culture flasks, allowing for the complete mixing of the 80 sccm odor flow with the 120 sccm of the dilution flow line's clean air. The air-volatiles mixture primed the line with volatiles up to the final valve, where the joint dilution + odor flow was directed towards the exhaust. Upon stimulus onset, the final valve redirected the fresh air flow to the exhaust and the dilution + odor flow via the stimulus flow line to the honeybee antennae. After 4 s of constant flow and stimulus delivery, the final valve redirected the fresh air flow via the stimulus flow line to the locust antenna and the dilution + odor flow back to the exhaust. One second after stimulus offset, the 80 sccm flowing through the odor flow line was redirected through the dilution flow line, mitigating any potential headspace depletion during the odor delivery. This protocol was designed to maintain a consistent flow rate through the stimulus flow line, thereby eliminating any potentially confounding neuronal responses due to mechanosensory detection of changes in air pressure. A 6″ diameter funnel pulling a slight vacuum was placed immediately behind the honeybee during odor delivery to ensure swift removal of odorants.

4.6. Electrophysiology

In vivo extracellular neural data for the putative cancer biomarkers and concentrations were collected from 34 to 19 honeybees, respectively. All cancer biomarker experiments were conducted using the same

stimulus panel made up of nine different VOCs and mineral oil. The biomarker concentration experiments were performed using a stimulus panel comprised of three varying concentrations (1% v/v, 0.01% v/v, and 0.0001% v/v) of two chemicals, hexanal and 2-methylheptane, for a total of six odors in addition to pure mineral oil as a control.

In vivo extracellular data for the synthetic breath mixtures were collected from 21 honeybees. For each experiment two separate panels of synthetic breath mixtures containing synthetic lung cancer patient breath, synthetic healthy patient breath, and mineral oil were created. The first panel was presented to the honeybees at two different times with a 10-min delay. The second panel, created using the exact same protocol, was then presented. Due to the extremely low concentrations in the mixtures, these synthetic breath odors were created fresh prior to every experiment.

The human lung cancer cell line data was collected from nine honeybees. The human lung cancer cell lines experiment comprised a panel with seven cultured lines and a media control. The cultured cell lines contained four NSCLC lines, two SCLC lines, and one healthy fibroblast control line.

The odor panels for each experiment were pseudorandomized prior to each recording, and each 4 s duration odor presentation was repeated five times with a 60 s inter-stimulus interval. This resulted in five trials of neural response data being collected for all odors of each odor panel (putative cancer biomarkers, descending concentrations, synthetic breath mixtures, and human lung cancer cell lines) presented to the insect. Each recording session lasted 1–2 h. Following surgery, a silver-chloride ground wire was placed into the ringer solution within the honeybee head capsule. Voltage signals from the ALNs were recorded by inserting a custom-made 4-channel electrode with impedance between 350 and 450 kΩ superficially into the center of the antennal lobe. Voltage signals were sampled at 20 kHz and then digitized using an Intan pre-amplifier board (C3334 RHD 16-channel headstage). The digitized signals were transmitted to the Intan recording controller (C3100 RHD USB interface board) prior to being visualized and stored using the Intan graphical user interface and LabView data acquisition system.

4.7. Spike sorting

All neural data was imported into MATLAB after high pass filtering using a 300Hz Butterworth filter. The data was analyzed by custom-written codes in MATLAB R2020b. For spike sorting analysis, all data was processed with Igor Pro using previously described methods and one to four channels (Pouzat et al., 2002). Detection thresholds for spiking events were between 2.5 and 3.5 standard deviations (SD) of baseline fluctuations. Single neurons were identified if they passed the following criteria: cluster separation $>$ 5 SD and inter-spike intervals (ISI) $<$ 20%. For the putative lung cancer biomarker panel, 44 neurons were identified from 34 honeybees. For the varying concentrations of two different lung cancer biomarkers, 45 neurons were identified from 19 honeybees. For the synthetic breath mixtures, 27 neurons were identified from 21 honeybees. For the lung cancer cell culture headspace odors, 27 neurons were identified from 9 honeybees. Spike sorted data was used for analyses in Figs. 1–3, 6, and Supplementary Figs. 2,3,5.

4.8. R.M.S. Transformation of neural voltage response

After importing the data into MATLAB and processing using the 300Hz filter, for R.M.S. analysis, large and wide voltage peaks, caused by palp movements, that were greater than 15 standard deviations from the mean voltage amplitude were removed by setting the 160 samples centered around each peak (8 ms duration) equal to the mean voltage value. This was done to remove any movement artifact from the data. For synthetic breath mixture analysis, out of a total of 1035 (23 positions x 3 odors $\times$ 3 odor panels x 5 trials = 1035) recorded R.M.S. responses, only 10 voltage traces (each with 1–2 artifacts per recording) contained this type of movement artifact. Next, the filtered data was trimmed to the time window of interest and passed through an R.M.S. filter as described in our previous work (Farnum et al., 2023). In short, a continuously moving 500-point R.M.S. filter, followed by a continuously moving 500-point averaging filter were applied to the raw voltage data. Baseline values calculated as the average of the 2 s prior to stimulus onset were subsequently subtracted from the data to obtain the ΔR.M.S. values. These ΔR.M.S. values were then binned into non-overlapping 10 ms or 50 ms bins and the average of each bin was computed. For the 23 recorded positions, obtained from the 21 honeybees, used for the synthetic breath mixture recordings (multiple recording positions from a single bee is possible), R.M.S. transformed voltage data from the 4-channels of the twisted wire electrode were averaged together. R.M.S. transformed data was used for analyses in Figs. 4 and 5.

4.9. Pairwise distance calculation

Using the binned spike sorted or binned R.M.S. data, the odor-evoked responses across all five trials for each neuron or R.M.S. position were averaged together. Then, all possible combinations of two different odors (45 combinations for 10 individual biomarkers and 3 combinations for 3 synthetic breath mixtures) were compared by calculating the absolute value of the difference between time-matched bins. The average of odor-evoked pairwise distances across all 44 neurons for the putative cancer biomarkers (Fig. 1d) and all 23 R.M.S. recording positions for the synthetic breath mixtures were also computed (Fig. 4e).

4.10. Dimensionality reduction analysis

We performed two methods of dimensionality reduction – Principal Component Analysis (PCA) and Linear Discriminant Analysis (LDA) as described in our previous study (Farnum et al., 2023). In PCA, we binned baseline subtracted, spike sorted neuronal signals into 50 ms non-overlapping time bins and averaged over trials ($n = 5$, each stimulus was repeated 5 times with a 1-min inter-stimulus interval). The baseline response was calculated for each neuron by averaging the firing rate over the 2 s time windows immediately before stimulus presentation across trials. Recorded neurons were pooled across multiple electrophysiology experiments. For example, in Fig. 1e, spike sorted and binned responses of all recorded neurons (44 total) were combined to generate a *neuron number (n = 44)* $\times$ *time bins (t = 10, number of* 50 ms *bins between* 250 ms – 750 ms*)* matrix, where each element in the matrix corresponds to the spike count of one neuron in one 50 ms time bin. Similar neuronal population time-series data matrices were generated for each stimulus. PCA dimensionality reduction analysis was performed on the time-series data involving all 10 putative cancer biomarkers and directions of maximum variance were found. The resultant high-dimensional vector in each time bin was projected along the principal component axes. Only three dimensions with the highest eigenvalues were considered for visualization purposes and data points in adjacent time bins were connected to generate low-dimensional neural trajectories. The same PCA analysis was applied to the varying concentrations of cancer biomarkers (Fig. 3c), synthetic breath mixtures (lung cancer, healthy, mineral oil) using the baseline subtracted R.M.S transformed population time-series data (Fig. 5b,c,d), and lung cancer cell culture odors (Fig. 6c). For LDA analysis, the same R.M.S transformed population time-series data matrix was used for synthetic breath mixtures and spike-sorted population matrix was used for varying concentrations of cancer biomarkers and lung cancer cell culture odors. Here, we maximized the separation between interclass distances while minimizing the within class distances. To visualize the data, time bins were plotted as unique points in this transformed LDA space and stimulus-specific VOC clusters became readily apparent (Fig. 5e,f,g, and Supplementary Figs. 2c, 3b, and 5c). All dimensionality reduction analyses were done using custom written MATLAB R2020b codes.

4.11. Quantitative classification: leave-one-trial-out

For individual biomarker classification, varying concentrations of biomarkers, and lung cancer cell culture odors, the spike sorted data was binned into 50 ms bins to create a three-dimensional matrix (e.g., 44 neurons × 5 trials × 10 time bins). The number of time bins depends on the time window of interest, for this analysis, the time window was chosen as 0.25–0.75 s after stimulus onset, which corresponds to the transient phase of the odor-evoked neural activity that is most discriminatory. For leave-one-trial-out (LOTO) analysis, four trials (out of total five) were averaged together to form a training template, while the fifth trial, the left-out trial, was used as the testing template. This was done for all odors to create as many training and testing templates as there were odors (e.g., for 10 odors there will be 10 training and 10 testing templates). For each time bin within the time window of interest, the Euclidean or Manhattan distance between the testing templates and the training templates were calculated and the testing templates were assigned based on the minimum Euclidean or Manhattan distance metric. Then, we iterated through the five trials, each time leaving out a different trial for the testing template and using the other four trials to create new training templates. The results are summarized with a confusion matrix (Fig. 2g). A fully diagonal matrix indicates 100% classification accuracy with any deviations indicating misclassifications. A further analysis was done by calculating the mode for each testing template across the 10 time bins in the time window of interest. The mode was used to classify the entire trial in a winner-take-all approach and the results are summarized in Fig. 2h, 3d and 6d. This same analysis was done on the R.M.S. transformed synthetic breath mixtures (Fig. 5h,i, j). Here, the three-dimensional matrix created for each odor is 23 positions × 5 trials × 10 time bins.

5. Conclusions

Our study demonstrates for the first time that a powerful biological VOC sensor, the honeybee olfactory brain, can be leveraged to detect human lung cancer biomarkers, complex mixtures of biomarkers at biological concentrations, and actual human lung cancer cell lines. By employing *in vivo* neural recordings from the honeybee brain as a noninvasive biosensing approach for lung cancer detection, we are able to combine the power of the entire biological olfactory sensory array (sensory neurons at the honeybee antennae), biological chemical transduction, and downstream neural network computations of the antennal lobe in one single brain-based VOC sensing device. We have also demonstrated that biological neural computational analyses can be performed on the odor-evoked neural data to achieve high classification success for synthetic lung cancer vs. healthy breath mixtures and for human lung cell lines healthy vs. NSCLC vs. SCLC. This novel study opens the door for more forward engineering approaches for cancer detection using honeybee olfactory neurons.

Code availability

All analyses were performed using custom written MATLAB codes. All codes are available from the corresponding author on request.

CRediT authorship contribution statement

Michael Parnas: Writing – review & editing, Writing – original draft, Visualization, Investigation, Formal analysis, Conceptualization. **Autumn K. McLane-Svoboda:** Writing – review & editing, Writing – original draft, Visualization, Investigation, Formal analysis, Data curation, Conceptualization. **Elyssa Cox:** Writing – review & editing, Writing – original draft, Methodology, Investigation, Conceptualization. **Summer B. McLane-Svoboda:** Writing – review & editing, Writing – original draft, Visualization, Investigation, Formal analysis. **Simon W. Sanchez:** Writing – review & editing, Writing – original draft, Visualization, Investigation, Formal analysis. **Alexander Farnum:** Methodology, Investigation. **Anthony Tundo:** Writing – review & editing, Methodology, Investigation. **Noël Lefevre:** Investigation, Formal analysis. **Sydney Miller:** Investigation. **Emily Neeb:** Investigation. **Christopher H. Contag:** Writing – review & editing, Supervision, Resources, Methodology. **Debajit Saha:** Writing – review & editing, Writing – original draft, Supervision, Resources, Project administration, Methodology, Funding acquisition, Conceptualization.

Declaration of competing interest

We wish to confirm that there are no known conflicts of interest associated with this publication and there has been no significant financial support for this work that could have influenced its outcome.

Data availability

Data will be made available on request.

Acknowledgements

This work was supported, in part, by an NSF CAREER [2238686] grant to D.S., Startup from Michigan State University to D.S., NSF Graduate Research Fellowship to A.M.S. and S.S, and the James and Kathleen Cornelius Endowment (C.H.C). We thank Dr. Gene E. Robinson (UIUC) for providing feedback on initial versions of the story, and Dr. Brian H. Smith (ASU) for advice on electrophysiology recordings and to facilitate supply of honeybees from Arizona to MSU.

Appendix A. Supplementary data

Supplementary data to this article can be found online at https://doi.org/10.1016/j.bios.2024.116466.

References

Ahn, J.H., et al., 2015. Screening of target-specific olfactory receptor and development of olfactory biosensor for the assessment of fungal contamination in grain. Sensor. Actuator. B Chem. 210, 9–16. https://doi.org/10.1016/j.snb.2014.12.060.

Altomare, D.F., et al., 2013. Exhaled volatile organic compounds identify patients with colorectal cancer. Br. J. Surg. 100, 144–150. https://doi.org/10.1002/bjs.8942.

Altomare, D.F., et al., 2020. Chemical signature of colorectal cancer: case–control study for profiling the breath print. BJS Open 4, 1189–1199. https://doi.org/10.1002/bjs5.50354.

Amal, H., et al., 2012. The scent fingerprint of hepatocarcinoma: in-vitro metastasis prediction with volatile organic compounds (VOCs). Int. J. Nanomed. 7, 4135–4146. https://doi.org/10.2147/ijn.S32680.

Amal, H., et al., 2015. Assessment of ovarian cancer conditions from exhaled breath. Int. J. Cancer 136, E614–E622. https://doi.org/10.1002/ijc.29166.

Amal, H., et al., 2016. Detection of precancerous gastric lesions and gastric cancer through exhaled breath. Gut 65, 400. https://doi.org/10.1136/gutjnl-2014-308536.

Amann, A., et al., 2014. The human volatilome: volatile organic compounds (VOCs) in exhaled breath, skin emanations, urine, feces and saliva. J. Breath Res. 8, 034001.

Amundsen, T., Sundstrøm, S., Buvik, T., Gederaas, O.A., Haaverstad, R., 2014. Can dogs smell lung cancer? First study using exhaled breath and urine screening in unselected patients with suspected lung cancer. Acta Oncol. 53, 307–315.

Anzivino, R., et al., 2022. The role of a polymer-based E-nose in the detection of head and neck cancer from exhaled breath. Sensors 22, 6485.

Arasaradnam, R.P., et al., 2014. Detection of colorectal cancer (CRC) by urinary volatile organic compound analysis. PLoS One 9, e108750. https://doi.org/10.1371/journal.pone.0108750.

Arasaradnam, R.P., et al., 2018. Noninvasive diagnosis of pancreatic cancer through Detection of volatile organic compounds in urine. Gastroenterology 154, 485–487. https://doi.org/10.1053/j.gastro.2017.09.054 e481.

Baldini, C., et al., 2020. Electronic nose as a novel method for diagnosing cancer: a systematic review. Biosensors 10. https://doi.org/10.3390/bios10080084.

Baldwin, D., Callister, M., 2016. What is the optimum screening strategy for the early detection of lung cancer. Clin. Oncol. 28, 672–681.

Bamji-Stocke, S., van Berkel, V., Miller, D.M., Frieboes, H.B., 2018. A review of metabolism-associated biomarkers in lung cancer diagnosis and treatment. Metabolomics 14, 81. https://doi.org/10.1007/s11306-018-1376-2.

Barash, O., et al., 2012. Classification of lung cancer histology by gold nanoparticle sensors. Nanomed. Nanotechnol. Biol. Med. 8, 580–589. https://doi.org/10.1016/j.nano.2011.10.001.

Barash, O., et al., 2015. Differentiation between genetic mutations of breast cancer by breath volatolomics. Oncotarget 6, 44864–44876. https://doi.org/10.18632/oncotarget.6269.
Binson, V., Subramoniam, M., 2022. Exhaled breath volatile organic compound analysis for the detection of lung cancer-A systematic review. Journal of Biomimetics, Biomaterials and Biomedical Engineering 56, 17–35.
Bitterman, M., Menzel, R., Fietz, A., Schäfer, S., 1983. Classical conditioning of proboscis extension in honeybees (Apis mellifera). J. Comp. Psychol. 97, 107.
Bortolotti, L., Costa, C., 2014. Chemical communication in the honey bee society. Neurobiology of Chemical Communication.
Brill, M.F., et al., 2013. Parallel processing via a dual olfactory pathway in the honeybee. J. Neurosci. 33, 2443–2456.
Brito, N.F., Moreira, M.F., Melo, A.C., 2016. A look inside odorant-binding proteins in insect chemoreception. J. Insect Physiol. 95, 51–65.
Brooks, S.W., Moore, D.R., Marzouk, E.B., Glenn, F.R., Hallock, R.M., 2015. Canine olfaction and electronic nose detection of volatile organic compounds in the detection of cancer: a review. Cancer Invest. 33, 411–419.
Broza, Y.Y., et al., 2019. Screening for gastric cancer using exhaled breath samples. Br. J. Surg. 106, 1122–1125. https://doi.org/10.1002/bjs.11294.
Brunner, C., et al., 2010. Discrimination of cancerous and non-cancerous cell lines by headspace-analysis with PTR-MS. Anal. Bioanal. Chem. 397, 2315–2324. https://doi.org/10.1007/s00216-010-3838-x.
Cave, J.W., Wickiser, J.K., Mitropoulos, A.N., 2019. Progress in the development of olfactory-based bioelectronic chemosensors. Biosens. Bioelectron. 123, 211–222. https://doi.org/10.1016/j.bios.2018.08.063.
Chang, J.-E., et al., 2018. Analysis of volatile organic compounds in exhaled breath for lung cancer diagnosis using a sensor system. Sensor. Actuator. B Chem. 255, 800–807. https://doi.org/10.1016/j.snb.2017.08.057.
Chen, J.-Y., et al., 2015. Learning modifies odor mixture processing to improve detection of relevant components. J. Neurosci. 35, 179–197.
Chen, Y., et al., 2016. Breath analysis based on surface-enhanced Raman scattering sensors distinguishes early and advanced gastric cancer patients from healthy persons. ACS Nano 10, 8169–8179. https://doi.org/10.1021/acsnano.6b01441.
Choueiry, F., Zhu, J., 2022. Secondary electrospray ionization-high resolution mass spectrometry (SESI-HRMS) fingerprinting enabled treatment monitoring of pulmonary carcinoma cells in real time. Anal. Chim. Acta 1189, 339230.
Chen, H., et al., 2021. COVID-19 screening using breath-borne volatile organic compounds. J. Breath Res. 15, 047104. https://doi.org/10.1088/1752-7163/ac2e57.
Choueiry, F., Barham, A., Zhu, J., 2022. Analyses of lung cancer-derived volatiles in exhaled breath and in vitro models. Exp. Biol. Med. 247, 1179–1190.
Cornu, J.-N., Cancel-Tassin, G., Ondet, V., Girardet, C., Cussenot, O., 2011. Olfactory detection of prostate cancer by dogs sniffing urine: a step forward in early diagnosis. Eur. Urol. 59, 197–201.
Dagogo-Jack, I., Shaw, A.T., 2018. Tumour heterogeneity and resistance to cancer therapies. Nat. Rev. Clin. Oncol. 15, 81–94.
Davies, M.P.A., et al., 2014. Unique volatolomic signatures of TP53 and KRAS in lung cells. Br. J. Cancer 111, 1213–1221. https://doi.org/10.1038/bjc.2014.411.
Van De Goor, R., Van Hooren, M., Dingemans, A.-M., Kremer, B., Kross, K., 2018. Training and validating a portable electronic nose for lung cancer screening. J. Thorac. Oncol. 13, 676–681. https://doi.org/10.1016/j.jtho.2018.01.024.
Díaz De León-Martínez, L., et al., 2020. Identification of profiles of volatile organic compounds in exhaled breath by means of an electronic nose as a proposal for a screening method for breast cancer: a case-control study. J. Breath Res. 14, 046009 https://doi.org/10.1088/1752-7163/aba83f.
Ehmann, R., et al., 2012. Canine scent detection in the diagnosis of lung cancer: revisiting a puzzling phenomenon. Eur. Respir. J. 39, 669–676.
Eigenbrodt, E., Kallinowski, F., Ott, M., Mazurek, S., Vaupel, P., 1998. Pyruvate kinase and the interaction of amino acid and carbohydrate metabolism in solid tumors. Anticancer Res. 18, 3267–3274.
Farnum, A., et al., 2023. Harnessing insect olfactory neural circuits for detecting and discriminating human cancers. Biosens. Bioelectron. 219, 114814 https://doi.org/10.1016/j.bios.2022.114814.
Filianoti, A., et al., 2022. Volatilome analysis in prostate cancer by electronic nose: a pilot monocentric study. Cancers 14, 2927.
Filipiak, W., et al., 2014. Comparative analyses of volatile organic compounds (VOCs) from patients, tumors and transformed cell lines for the validation of lung cancer-derived breath markers. J. Breath Res. 8, 027111.
Fonta, C., Sun, X.-J., Masson, C., 1993. Morphology and spatial distribution of bee antennal lobe interneurones responsive to odours. Chem. Senses 18, 101–119.
Fuchs, P., Loeseken, C., Schubert, J.K., Miekisch, W., 2010. Breath gas aldehydes as biomarkers of lung cancer. Int. J. Cancer 126, 2663–2670.
Furuhashi, T., Ishii, R., Onishi, H., Ota, S., 2020. Elucidation of biochemical pathways underlying VOCs production in A549 cells. Front. Mol. Biosci. 7 https://doi.org/10.3389/fmolb.2020.00116.
van Geffen, W.H., et al., 2019. The electronic nose: emerging biomarkers in lung cancer diagnostics. Breathe 15, e135–e141.
Gentric, G., Mieulet, V., Mechta-Grigoriou, F., 2017. Heterogeneity in cancer metabolism: new concepts in an old field. Antioxidants Redox Signal. 26, 462–485.
van de Goor, R.M.G.E., et al., 2017. Feasibility of electronic nose technology for discriminating between head and neck, bladder, and colon carcinomas. Eur. Arch. Oto-Rhino-Laryngol. 274, 1053–1060. https://doi.org/10.1007/s00405-016-4320-y.
Gordon, R.T., et al., 2008. The use of canines in the detection of human cancers. J. Alternative Compl. Med. 14, 61–67.
Goto, T., Hirotsu, Y., Amemiya, K., Mochizuki, H., Omata, M., 2018. Understanding intratumor heterogeneity and evolution in NSCLC and potential new therapeutic approach. Cancers 10, 212.
Gouzerh, F., et al., 2022. Odors and cancer: current status and future directions. Biochim. Biophys. Acta Rev. Canc 1877, 188644. https://doi.org/10.1016/j.bbcan.2021.188644.
Gower, H., et al., 2023. Potential role of volatile organic compound breath testing in the Australasian colorectal cancer pathway. ANZ J. Surg. 93 (5), 1159–1161.
Groh, C., Rössler, W., 2020. Analysis of synaptic microcircuits in the mushroom bodies of the honeybee. Insects 11, 43.
Gruber, M., et al., 2014. Analysis of exhaled breath for diagnosing head and neck squamous cell carcinoma: a feasibility study. Br. J. Cancer 111, 790–798.
Guo, L., et al., 2015. Exhaled breath volatile biomarker analysis for thyroid cancer. Transl. Res. 166, 188–195. https://doi.org/10.1016/j.trsl.2015.01.005.
Haick, H., Broza, Y.Y., Mochalski, P., Ruzsanyi, V., Amann, A., 2014. Assessment, origin, and implementation of breath volatile cancer markers. Chem. Soc. Rev. 43, 1423–1449. https://doi.org/10.1039/c3cs60329f.
Hakim, M., et al., 2011. Diagnosis of head-and-neck cancer from exhaled breath. Br. J. Cancer 104, 1649–1655. https://doi.org/10.1038/bjc.2011.128.
He, J., et al., 2014. Fingerprinting breast cancer vs. Normal mammary cells by mass spectrometric analysis of volatiles. Sci. Rep. 4, 5196. https://doi.org/10.1038/srep05196.
Horváth, I., Lázár, Z., Gyulai, N., Kollai, M., Losonczy, G., 2009. Exhaled biomarkers in lung cancer. Eur. Respir. J. 34, 261–275. https://doi.org/10.1183/09031936.00142508.
Horvath, G., Andersson, H., Paulsson, G., 2011. Characteristic odour in the blood reveals ovarian carcinoma. EUROMEDICA 67.
Hurot, C., Scaramozzino, N., Buhot, A., Hou, Y., 2020. Bio-inspired strategies for improving the selectivity and sensitivity of artificial noses: a review. Sensors 20. https://doi.org/10.3390/s20061803.
Iqbal, M.J., et al., 2022. Biosensing chips for cancer diagnosis and treatment: a new wave towards clinical innovation. Cancer Cell Int. 22, 354.
Janssens, E., et al., 2022. Headspace volatile organic compound profiling of pleural mesothelioma and lung cancer cell lines as translational bridge for breath research. Front. Oncol. 12.
Jia, Z., et al., 2018. Detection of lung cancer: concomitant volatile organic compounds and metabolomic profiling of six cancer cell lines of different histological origins. ACS Omega 3, 5131–5140. https://doi.org/10.1021/acsomega.7b02035.
Jia, Z., Patra, A., Kutty, V.K., Venkatesan, T., 2019. Critical review of volatile organic compound analysis in breath and in vitro cell culture for detection of lung cancer. Metabolites 9. https://doi.org/10.3390/metabo9030052.
Jin, H.J., et al., 2012. Nanovesicle-based bioelectronic nose platform mimicking human olfactory signal transduction. Biosens. Bioelectron. 35, 335–341. https://doi.org/10.1016/j.bios.2012.03.012.
Joerges, J., Küttner, A., Galizia, C.G., Menzel, R., 1997. Representations of odours and odour mixtures visualized in the honeybee brain. Nature 387, 285–288.
Kaloumenou, M., Skotadis, E., Lagopati, N., Efstathopoulos, E., Tsoukalas, D., 2022. Breath analysis: a promising tool for disease diagnosis-the role of sensors. Sensors 22. https://doi.org/10.3390/s22031238.
Karakaya, D., Ulucan, O., Turkan, M., 2020. Electronic nose and its applications: a survey. Int. J. Autom. Comput. 17, 179–209. https://doi.org/10.1007/s11633-019-1212-9.
van Keulen, K.E., Jansen, M.E., Schrauwen, R.W.M., Kolkman, J.J., Siersema, P.D., 2020. Volatile organic compounds in breath can serve as a non-invasive diagnostic biomarker for the detection of advanced adenomas and colorectal cancer. Aliment. Pharmacol. Ther. 51, 334–346. https://doi.org/10.1111/apt.15622.
Ko, H.J., Park, T.H., 2016. Bioelectronic nose and its application to smell visualization. J. Biol. Eng. 10 (17) https://doi.org/10.1186/s13036-016-0041-4.
Kononov, A., et al., 2019. Online breath analysis using metal oxide semiconductor sensors (electronic nose) for diagnosis of lung cancer. J. Breath Res. 14, 016004 https://doi.org/10.1088/1752-7163/ab433d.
Kontos, E., et al., 2022. Bees can be trained to identify SARS-CoV-2 infected samples. Biol. Open 11 (4), bio059111.
Koureas, M., et al., 2020. Target analysis of volatile organic compounds in exhaled breath for lung cancer discrimination from other pulmonary diseases and healthy persons. Metabolites 10. https://doi.org/10.3390/metabo10080317.
Kowalczyk, T., et al., 2021. The ability of metabolomics to discriminate non-small-cell lung cancer subtypes depends on the stage of the disease and the type of material studied. Cancers 13, 3314.
Krauss, E., et al., 2020. Recognition of breathprints of lung cancer and chronic obstructive pulmonary disease using the Aeonose® electronic nose. J. Breath Res. 14, 046004 https://doi.org/10.1088/1752-7163/ab8c50.
Krofczik, S., Menzel, R., Nawrot, M.P., 2009. Rapid odor processing in the honeybee antennal lobe network. Front. Comput. Neurosci. 2, 287.
Kunte, S., Abraham, J., Montero, A.J., 2020. Novel HER2–targeted therapies for HER2–positive metastatic breast cancer. Cancer 126, 4278–4288.
Larisika, M., et al., 2015. Electronic olfactory sensor based on A. mellifera odorant-binding protein 14 on a reduced graphene oxide field-effect transistor. Angew. Chem. Int. Ed. 54, 13245–13248. https://doi.org/10.1002/anie.201505712.
Lavra, L., et al., 2015. Investigation of VOCs associated with different characteristics of breast cancer cells. Sci. Rep. 5, 13246 https://doi.org/10.1038/srep13246.
Lee, S.H., Oh, E.H., Park, T.H., 2015. Cell-based microfluidic platform for mimicking human olfactory system. Biosens. Bioelectron. 74, 554–561. https://doi.org/10.1016/j.bios.2015.06.072.

Lim, J.H., et al., 2014. Nanovesicle-based bioelectronic nose for the diagnosis of lung cancer from human blood. Adv. Healthcare Mater. 3, 360–366. https://doi.org/10.1002/adhm.201300174.
Lim, S.L., et al., 2018. Metabolic signatures of four major histological types of lung cancer cells. Metabolomics 14, 118. https://doi.org/10.1007/s11306-018-1417-x.
Lima, A.R., et al., 2018. Discrimination between the human prostate normal and cancer cell exometabolome by GC-MS. Sci. Rep. 8, 5539. https://doi.org/10.1038/s41598-018-23847-9.
Lu, Y., et al., 2014. Olfactory biosensor using odorant-binding proteins from honeybee: ligands of floral odors and pheromones detection by electrochemical impedance. Sensor. Actuator. B Chem. 193, 420–427. https://doi.org/10.1016/j.snb.2013.11.045.
Lüdke, A., Galizia, C.G., 2014. Sniffing cancer: will the fruit fly beat the dog? ChemoSense 15, 3–15.
Ma, P., et al., 2023. Non-invasive exhaled breath diagnostic and monitoring technologies. Microw. Opt. Technol. Lett. 65, 1475–1488.
MaBouDi, H., Shimazaki, H., Giurfa, M., Chittka, L., 2017. Olfactory learning without the mushroom bodies: spiking neural network models of the honeybee lateral antennal lobe tract reveal its capacities in odour memory tasks of varied complexities. PLoS Comput. Biol. 13, e1005551.
Maeda, J., et al., 2010. Possibility of multivariate function composed of plasma amino acid profiles as a novel screening index for non-small cell lung cancer: a case control study. BMC Cancer 10, 1–8.
Manzini, I., Schild, D., Di Natale, C., 2021. Principles of odor coding in vertebrates and artificial chemosensory systems. Physiol. Rev. 102, 61–154. https://doi.org/10.1152/physrev.00036.2020.
McCulloch, M., et al., 2006. Diagnostic accuracy of canine scent detection in early-and late-stage lung and breast cancers. Integr. Cancer Ther. 5, 30–39.
Mendes, C., et al., 2023. NSCLC presents metabolic heterogeneity, and there is still some leeway for EGF stimuli in EGFR-mutated NSCLC. Lung Cancer 182, 107283.
Mgode, G.F., et al., 2012. Diagnosis of tuberculosis by trained African giant pouched rats and confounding impact of pathogens and microflora of the respiratory tract. J. Clin. Microbiol. 50, 274–280.
Misawa, N., Mitsuno, H., Kanzaki, R., Takeuchi, S., 2010. Highly sensitive and selective odorant sensor using living cells expressing insect olfactory receptors. Proc. Natl. Acad. Sci. USA 107, 15340–15344. https://doi.org/10.1073/pnas.1004334107.
Mochalski, P., et al., 2013. Release and uptake of volatile organic compounds by human hepatocellular carcinoma cells (HepG2) in vitro. Cancer Cell Int. 13, 72. https://doi.org/10.1186/1475-2867-13-72.
Mochalski, P., et al., 2018. Ex vivo emission of volatile organic compounds from gastric cancer and non-cancerous tissue. J. Breath Res. 12, 046005.
Moreno, E., Corriale, M.J., Arenas, A., 2022. Differences in olfactory sensitivity and odor detection correlate with foraging task specialization in honeybees Apis mellifera. J. Insect Physiol. 141, 104416.
Nardi-Agmon, I., Peled, N., 2017. Exhaled breath analysis for the early detection of lung cancer: recent developments and future prospects. Lung Cancer 8, 31–38. https://doi.org/10.2147/lctt.S104205.
Neta, S., Ariel, G., Yossi, Y., Amir, A., Ben, M.M., 2023. The Locust antenna as an odor discriminator. Biosens. Bioelectron. 221, 114919.
Niemi, R.J., et al., 2018. FAIMS analysis of urine gaseous headspace is capable of differentiating ovarian cancer. Gynecol. Oncol. 151, 519–524. https://doi.org/10.1016/j.ygyno.2018.09.016.
Oudkerk, M., Liu, S., Heuvelmans, M.A., Walter, J.E., Field, J.K., 2021. Lung cancer LDCT screening and mortality reduction—evidence, pitfalls and future perspectives. Nat. Rev. Clin. Oncol. 18, 135–151.
Panicker, L.R., et al., 2023. Trends and challenges in electroanalytical biosensing methodologies for infectious viral diseases. Bioelectrochemistry 108594.
Paoli, M., Galizia, G.C., 2021. Olfactory coding in honeybees. Cell Tissue Res. 383, 35–58.
Pedersen, S., et al., 2021. Identifying metabolic alterations in newly diagnosed small cell lung cancer patients. Metabolism Open 12, 100127. https://doi.org/10.1016/j.metop.2021.100127.
Peled, N., et al., 2013. Volatile fingerprints of cancer specific genetic mutations. Nanomed. Nanotechnol. Biol. Med. 9, 758–766. https://doi.org/10.1016/j.nano.2013.01.008.
Peng, G., et al., 2009. Diagnosing lung cancer in exhaled breath using gold nanoparticles. Nat. Nanotechnol. 4, 669–673. https://doi.org/10.1038/nnano.2009.235.
Peng, G., et al., 2010a. Detection of lung, breast, colorectal, and prostate cancers from exhaled breath using a single array of nanosensors. Br. J. Cancer 103, 542–551. https://doi.org/10.1038/sj.bjc.6605810.
Peng, G., et al., 2010b. Detection of lung, breast, colorectal, and prostate cancers from exhaled breath using a single array of nanosensors. Br. J. Cancer 103, 542–551. https://doi.org/10.1038/sj.bjc.6605810.
Pereira, J., et al., 2015a. Breath analysis as a potential and non-invasive frontier in disease diagnosis: an overview. Metabolites 5, 3–55. https://doi.org/10.3390/metabo5010003.
Pereira, J., et al., 2015b. Breath analysis as a potential and non-invasive frontier in disease diagnosis: an overview. Metabolites 5, 3–55. https://doi.org/10.3390/metabo5010003.
Perez-Orive, J., et al., 2002. Oscillations and sparsening of odor representations in the mushroom body. Science 297, 359–365.
Phillips, M., et al., 1999. Volatile organic compounds in breath as markers of lung cancer: a cross-sectional study. Lancet 353, 1930–1933. https://doi.org/10.1016/s0140-6736(98)07552-7.
Phillips, M., et al., 2003. Volatile markers of breast cancer in the breath. Breast J. 9, 184–191. https://doi.org/10.1046/j.1524-4741.2003.09309.x.
Phillips, M., et al., 2006. Prediction of breast cancer using volatile biomarkers in the breath. Breast Cancer Res. Treat. 99, 19–21. https://doi.org/10.1007/s10549-006-9176-1.
Phillips, M., Bevers, T.B., Larsen, L.H., Pappas, N., Pathak, S., 2020. Rapid point-of-care breath test predicts breast cancer and abnormal mammograms in symptomatic women. medRxiv, 20042895, 2020.2004. 2007.
Pickel, D., Manucy, G.P., Walker, D.B., Hall, S.B., Walker, J.C., 2004. Evidence for canine olfactory detection of melanoma. Appl. Anim. Behav. Sci. 89, 107–116.
Piqueret, B., et al., 2022. Ants detect cancer cells through volatile organic compounds. iScience 25, 103959. https://doi.org/10.1016/j.isci.2022.103959.
Pisters, P.W., Pearlstone, D.B., Toroslan, M., 1993. Protein and amino acid metabolism in cancer cachexia: investigative techniques and therapeutic interventions. Crit. Rev. Clin. Lab Sci. 30, 223–272.
Poli, D., et al., 2005. Exhaled volatile organic compounds in patients with non-small cell lung cancer: cross sectional and nested short-term follow-up study. Respir. Res. 6, 71. https://doi.org/10.1186/1465-9921-6-71.
Poli, D., et al., 2010. Determination of aldehydes in exhaled breath of patients with lung cancer by means of on-fiber-derivatisation SPME–GC/MS. J. Chromatogr. B 878, 2643–2651.
Popov, T.A., 2011. Human exhaled breath analysis. Ann. Allergy Asthma Immunol. 106, 451–456.
Pouzat, C., Mazor, O., Laurent, G., 2002. Using noise signature to optimize spike-sorting and to assess neuronal classification quality. J. Neurosci. Methods 122, 43–57. https://doi.org/10.1016/s0165-0270(02)00276-5.
Puchades-Carrasco, L., et al., 2016. Serum metabolomic profiling facilitates the non-invasive identification of metabolic biomarkers associated with the onset and progression of non-small cell lung cancer. Oncotarget 7, 12904.
Queralto, N., et al., 2014. Detecting cancer by breath volatile organic compound analysis: a review of array-based sensors. J. Breath Res. 8, 027112.
Raman, B., Joseph, J., Tang, J., Stopfer, M., 2010. Temporally diverse firing patterns in olfactory receptor neurons underlie spatiotemporal neural codes for odors. J. Neurosci. 30, 1994–2006. https://doi.org/10.1523/jneurosci.5639-09.2010.
Raspagliesi, F., et al., 2020. Detection of ovarian cancer through exhaled breath by electronic nose: a prospective study. Cancers 12. https://doi.org/10.3390/cancers12092408.
Ratiu, I.A., Ligor, T., Bocos-Bintintan, V., Mayhew, C.A., Buszewski, B., 2020. Volatile organic compounds in exhaled breath as fingerprints of lung cancer, asthma and COPD. J. Clin. Med. 10, 32.
Reinhard, J., Sinclair, M., Srinivasan, M.V., Claudianos, C., 2010. Honeybees learn odour mixtures via a selection of key odorants. PLoS One 5, e9110.
Robertson, H.M., Wanner, K.W., 2006. The chemoreceptor superfamily in the honey bee, Apis mellifera: expansion of the odorant, but not gustatory, receptor family. Genome Res. 16, 1395–1403.
Röck, F., Barsan, N., Weimar, U., 2008. Electronic nose: current status and future trends. Chem. Rev. 108, 705–725. https://doi.org/10.1021/cr068121q.
Roine, A., et al., 2014. Detection of prostate cancer by an electronic nose: a proof of principle study. J. Urol. 192, 230–235. https://doi.org/10.1016/j.juro.2014.01.113.
Sachse, S., Rappert, A., Galizia, C.G., 1999. The spatial representation of chemical structures in the antennal lobe of honeybees: steps towards the olfactory code. Eur. J. Neurosci. 11, 3970–3982.
Saha, D., et al., 2013a. A spatiotemporal coding mechanism for background-invariant odor recognition. Nat. Neurosci. 16, 1830–1839. https://doi.org/10.1038/nn.3570.
Saha, D., Leong, K., Katta, N., Raman, B., 2013b. Multi-unit recording methods to characterize neural activity in the locust (Schistocerca americana) olfactory circuits. J. Vis. Exp. https://doi.org/10.3791/50139.
Saha, D., et al., 2015. Behavioural correlates of combinatorial versus temporal features of odour codes. Nat. Commun. 6, 6953. https://doi.org/10.1038/ncomms7953.
Saha, D., et al., 2017. Engaging and disengaging recurrent inhibition coincides with sensing and unsensing of a sensory stimulus. Nat. Commun. 8, 15413 https://doi.org/10.1038/ncomms15413.
Saha, D., et al., 2020. Explosive sensing with insect-based biorobots. Biosens. Bioelectron. X 6, 100050. https://doi.org/10.1016/j.biosx.2020.100050.
Saidi, T., et al., 2020. Non-invasive prediction of lung cancer histological types through exhaled breath analysis by UV-irradiated electronic nose and GC/QTOF/MS. Sensor. Actuator. B Chem. 311, 127932 https://doi.org/10.1016/j.snb.2020.127932.
Sandoz, J.C., 2011. Behavioral and neurophysiological study of olfactory perception and learning in honeybees. Front. Syst. Neurosci. 5, 98.
Sankaran, S., Panigrahi, S., Mallik, S., 2011. Odorant binding protein based biomimetic sensors for detection of alcohols associated with Salmonella contamination in packaged beef. Biosens. Bioelectron. 26, 3103–3109. https://doi.org/10.1016/j.bios.2010.07.122.
Schallschmidt, K., et al., 2016. Comparison of volatile organic compounds from lung cancer patients and healthy controls—challenges and limitations of an observational study. J. Breath Res. 10, 046007.
Scheepers, M.H.M.C., et al., 2022. Diagnostic performance of electronic noses in cancer diagnoses using exhaled breath: a systematic review and meta-analysis. JAMA Netw. Open 5, e2219372. https://doi.org/10.1001/jamanetworkopen.2022.19372.
Serasanambati, M., Broza, Y.Y., Haick, H., 2019a. Volatile compounds are involved in cellular crosstalk and upregulation. Advanced Biosystems 3, 1900131. https://doi.org/10.1002/adbi.201900131.
Serasanambati, M., Broza, Y.Y., Marmur, A., Haick, H., 2019b. Profiling single cancer cells with volatolomics approach. iScience 11, 178–188. https://doi.org/10.1016/j.isci.2018.12.008.
Sertorio, M., et al., 2018. Cancer cell metabolism: implications for X-ray and particle radiation therapy. International Journal of Particle Therapy 5, 40–48. https://doi.org/10.14338/IJPT-18-00023.1.

Shehada, N., et al., 2015. Ultrasensitive silicon nanowire for real-world gas sensing: noninvasive diagnosis of cancer from breath volatolome. Nano Lett. 15, 1288–1295. https://doi.org/10.1021/nl504482t.
Shirasu, M., Touhara, K., 2011. The scent of disease: volatile organic compounds of the human body related to disease and disorder. J. Biochem. 150, 257–266.
Silva, C.L., Perestrelo, R., Silva, P., Tomás, H., Câmara, J.S., 2017. Volatile metabolomic signature of human breast cancer cell lines. Sci. Rep. 7, 43969 https://doi.org/10.1038/srep43969.
Španěl, P., Smith, D., 2020. Quantification of volatile metabolites in exhaled breath by selected ion flow tube mass spectrometry, SIFT-MS. Clin Mass Spectrom 16, 18–24. https://doi.org/10.1016/j.clinms.2020.02.001.
Sponring, A., et al., 2010. Analysis of volatile organic compounds (VOCs) in the headspace of NCI-H1666 lung cancer cells. Cancer Biomarkers 7, 153–161. https://doi.org/10.3233/CBM-2010-0182.
Staal-van den Brekel, A.J., et al., 1997. Metabolism in patients with small cell lung carcinoma compared with patients with non-small cell lung carcinoma and healthy controls. Thorax 52, 338–341.
Stopfer, M., 2014. Central processing in the mushroom bodies. Current Opinion in Insect Science 6, 99–103. https://doi.org/10.1016/j.cois.2014.10.009.
Stopfer, M., Laurent, G., 1999. Short-term memory in olfactory network dynamics. Nature 402, 664–668.
Stopfer, M., Bhagavan, S., Smith, B.H., Laurent, G., 1997. Impaired odour discrimination on desynchronization of odour-encoding neural assemblies. Nature 390, 70–74.
Stopfer, M., Jayaraman, V., Laurent, G., 2003. Intensity versus identity coding in an olfactory system. Neuron 39, 991–1004. https://doi.org/10.1016/j.neuron.2003.08.011.
Strauch, M., et al., 2014. More than apples and oranges-Detecting cancer with a fruit fly's antenna. Sci. Rep. 4, 1–9.
Suckling, D.M., Sagar, R.L., 2011. Honeybees Apis mellifera can detect the scent of Mycobacterium tuberculosis. Tuberculosis 91, 327–328.
Sung, H., et al., 2021. Global cancer statistics 2020: GLOBOCAN estimates of incidence and mortality worldwide for 36 cancers in 185 countries. CA A Cancer J. Clin. 71, 209–249.
Tang, H., et al., 2017. Determination of volatile organic compounds exhaled by cell lines derived from hematological malignancies. Biosci. Rep. 37, BSR20170106 https://doi.org/10.1042/BSR20170106.
Thriumani, R., et al., 2016. A study on VOCs released by lung cancer cell line using GCMS-SPME. Procedia Chem. 20, 1–7. https://doi.org/10.1016/j.proche.2016.07.027.
Thriumani, R., et al., 2018. A study on volatile organic compounds emitted by in-vitro lung cancer cultured cells using gas sensor array and SPME-GCMS. BMC Cancer 18, 362. https://doi.org/10.1186/s12885-018-4235-7.
Tiele, A., Wicaksono, A., Kansara, J., Arasaradnam, R.P., Covington, J.A., 2019. Breath analysis using eNose and ion mobility technology to diagnose inflammatory bowel disease-A pilot study. Biosensors 9. https://doi.org/10.3390/bios9020055.
Tiele, A., et al., 2020. Breath-based non-invasive diagnosis of Alzheimer's disease: a pilot study. J. Breath Res. 14, 026003 https://doi.org/10.1088/1752-7163/ab6016.
Urbanová, L., Vyhnánková, V., Krisová, Š., Pacík, D., Nečas, A., 2015. Intensive training technique utilizing the dog's olfactory abilities to diagnose prostate cancer in men. Acta Vet. 84.
Va, B., Subramoniam, M., Mathew, L., 2021. Noninvasive detection of COPD and Lung Cancer through breath analysis using MOS Sensor array based e-nose. Expert Rev. Mol. Diagn. 21, 1223–1233.
Vidic, J., et al., 2007. Gold surface functionalization and patterning for specific immobilization of olfactory receptors carried by nanosomes. Anal. Chem. 79, 3280–3290. https://doi.org/10.1021/ac061774m.
Waltman, C.G., Marcelissen, T.A.T., van Roermund, J.G.H., 2020. Exhaled-breath testing for prostate cancer based on volatile organic compound profiling using an electronic nose device (Aeonose™): a preliminary report. European Urology Focus 6, 1220–1225. https://doi.org/10.1016/j.euf.2018.11.006.
Wang, C., et al., 2014. Volatile organic metabolites identify patients with breast cancer, cyclomastopathy and mammary gland fibroma. Sci. Rep. 4, 5383. https://doi.org/10.1038/srep05383.
Weetjens, B., et al., 2009. African pouched rats for the detection of pulmonary tuberculosis in sputum samples. Int. J. Tubercul. Lung Dis. 13, 737–743.
Williams, H., Pembroke, A., 1989. Sniffer dogs in the melanoma clinic? Lancet 333, 734.
Willis, C.M., et al., 2004a. Olfactory detection of human bladder cancer by dogs: proof of principle study. BMJ 329, 712. https://doi.org/10.1136/bmj.329.7468.712.
Willis, C.M., et al., 2004b. Olfactory detection of human bladder cancer by dogs: proof of principle study. Br. Med. J. 329, 712.
Willis, C.M., Britton, L.E., Harris, R., Wallace, J., Guest, C.M., 2011. Volatile organic compounds as biomarkers of bladder cancer: sensitivity and specificity using trained sniffer dogs. Cancer Biomarkers 8, 145–153.
Wu, T.-Z., 1999. A piezoelectric biosensor as an olfactory receptor for odour detection: electronic nose. Biosens. Bioelectron. 14, 9–18. https://doi.org/10.1016/S0956-5663(98)00086-4.
Xiang, L., Wu, S., Hua, Q., Bao, C., Liu, H., 2021. Volatile organic compounds in human exhaled breath to diagnose gastrointestinal cancer: a meta-analysis. Front. Oncol. 11, 606915.
Xu, Z., et al., 2013. A nanomaterial-based breath test for distinguishing gastric cancer from benign gastric conditions. Br. J. Cancer 108, 941–950.
Yang, Y., Krieger, J., Zhang, L., Breer, H., 2012. The olfactory co-receptor Orco from the migratory locust (Locusta migratoria) and the desert locust (Schistocerca gregaria): identification and expression pattern. Int. J. Biol. Sci. 8, 159.
Yang, H., et al., 2017. Nanodisc-based bioelectronic nose using olfactory receptor produced in Escherichia coli for the assessment of the death-associated odor cadaverine. ACS Nano 11, 11847–11855. https://doi.org/10.1021/acsnano.7b04992.
Zhang, Y., et al., 2014. Identification of volatile biomarkers of gastric cancer cells and ultrasensitive electrochemical detection based on sensing interface of Au-Ag alloy coated MWCNTs. Theranostics 4, 154–162. https://doi.org/10.7150/thno.7560.
Zhou, W., et al., 2012. Proteomic analysis reveals Warburg effect and anomalous metabolism of glutamine in pancreatic cancer cells. J. Proteome Res. 11, 554–563.